
nuReasoning: A Reasoning-Centric Dataset and Benchmark for Long-Tail Autonomous Driving

Zhiyu Huang^{1*} Johnson Liu^{1*} Rui Song^{1*} Zewei Zhou^{1,2} Ruining Yang²
Yun Zhang¹ Tianhui Cai¹ Hanyin Zhang¹ Mingxuan Gao¹ Valeria Xu¹
Jiali Chen¹ Yishan Shen² Yiluan Guo² Tony (Xuewei) Qi^{2†} Jiaqi Ma¹

¹University of California, Los Angeles ²Motional

<https://nureasoning.github.io/>

Abstract

Reasoning is essential for autonomous driving (AD) in long-tail scenarios, where vehicles must apply commonsense knowledge, understand spatial relations, infer agent interactions, and make safe decisions. However, existing AD datasets and benchmarks mainly target perception, prediction, or planning, and provide limited supervision for reasoning over realistic long-tail driving scenes. We introduce **nuReasoning**, a large-scale real-world dataset and benchmark for reasoning-centric AD. Following the lineage of nuScenes and nuPlan, nuReasoning advances real-world AD datasets and benchmarks toward reasoning in long-tail driving scenarios. The dataset contains 20,000 clips, each 20 seconds long, collected across multiple cities, with synchronized multi-camera images, LiDAR data, HD maps, object annotations, and human-verified reasoning annotations spanning *Spatial Reasoning*, *Decision Reasoning*, and *Counterfactual Reasoning*. Unlike prior datasets that focus primarily on visual question answering, nuReasoning supports both reasoning evaluation and planning evaluation, enabling a direct study of how reasoning supervision affects driving performance. Experiments show that fine-tuning VLMs on nuReasoning substantially improves driving-specific question answering, while incorporating reasoning supervision into VLA training improves planning performance even when textual reasoning outputs are disabled at inference time. These results establish nuReasoning as a foundation for evaluating and improving robust, interpretable, reasoning-driven AD systems in realistic long-tail settings.

1 Introduction

Autonomous driving (AD) has advanced rapidly over the past decade, driven by progress in perception, prediction, and planning [1–11]. Recently, end-to-end methods have emerged as a dominant paradigm by directly mapping sensor inputs to driving actions within a unified framework [12–21]. However, most end-to-end systems are still primarily trained through expert trajectory imitation, which can limit their ability to generalize to rare, unseen, and long-tail scenarios that require deeper scene understanding and reasoning. Generative AI provides a new opportunity to build more capable and interpretable AD systems [22]. Vision-language models (VLMs) have shown strong potential for perception, semantic understanding, and visual reasoning [23–31], while vision-language-action (VLA) models extend these capabilities to decision-making and planning [32–41]. A central promise of these models is **reasoning**: inferring spatial relationships, interpreting agent intent, understanding scene context, anticipating consequences, and making informed decisions in complex environments.

*Equal contribution.

†Project lead. Corresponding author. Contact: qixuewei@gmail.com

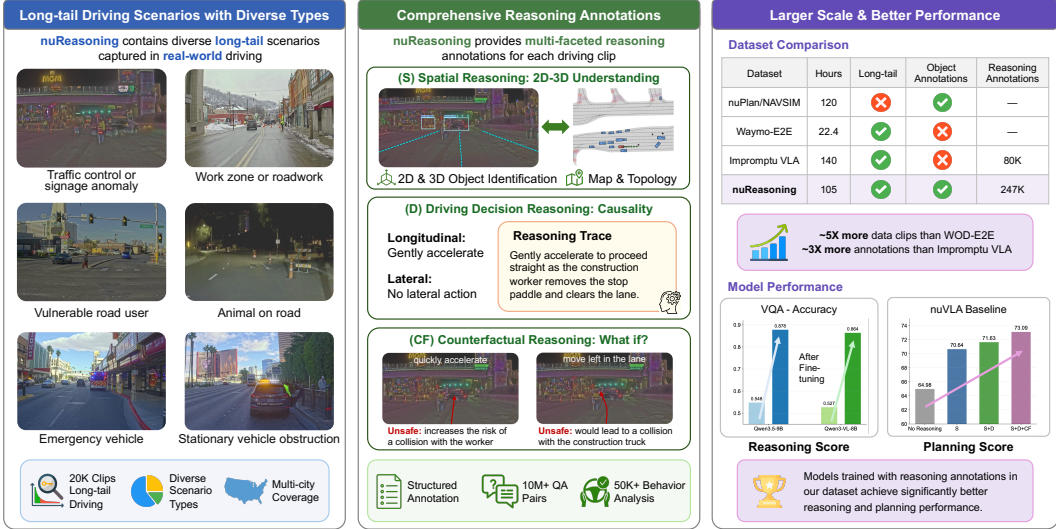


Figure 1: **nuReasoning** is a large-scale real-world long-tail driving dataset containing 20K 20-second clips across diverse scenario types. The dataset provides high-quality reasoning annotations spanning spatial reasoning, driving decisions, and counterfactual reasoning. Compared with prior datasets, nuReasoning offers substantially larger-scale long-tail driving data and richer reasoning annotations, enabling models trained on it to achieve significantly improved reasoning and planning performance.

However, reasoning remains underdeveloped in current AD systems, largely because existing datasets and benchmarks provide limited supervision and evaluation for reasoning in realistic driving scenarios.

Existing AD datasets and benchmarks mainly target perception [42, 43], trajectory prediction [44–46], or planning [47–50]. While these datasets have been essential for AD research, they provide limited support for reasoning-centric learning. Recent datasets introduce VLM-oriented reasoning tasks [24, 51–55], but typically focus on question answering and do not evaluate downstream planning. VLA datasets [56, 57] are often built from routine driving data and provide limited coverage of long-tail, reasoning-intensive cases. Moreover, existing annotations are usually narrow in scope, emphasizing scene descriptions while lacking spatial-temporal, causal, and counterfactual reasoning. Consequently, current VLA systems remain brittle in long-tail scenarios and struggle with multi-view, temporal, and causal understanding [29, 58–61].

To address these limitations, we introduce **nuReasoning**, a large-scale real-world dataset and benchmark for reasoning and end-to-end learning in AD. Following the dataset and benchmark lineage of *nuScenes* [42] and *nuPlan* [47, 62], nuReasoning extends this ecosystem from perception and planning toward reasoning-centric autonomous driving. The dataset contains 20K real-world driving clips, each 20 seconds long at 10 Hz, mined from large-scale driving logs to maximize scenario diversity and difficulty. Each clip includes synchronized multi-modal inputs, including multi-camera images, LiDAR, HD maps, and object annotations, together with three complementary reasoning annotations: *Spatial Reasoning*, *Decision Reasoning*, and *Counterfactual Reasoning*. These annotations are produced by automated context-aware pipelines and validated by human experts to ensure scalability and quality. Based on this dataset, the **nuReasoning Benchmark** evaluates both reasoning accuracy and planning performance, providing a unified testbed for VLM and VLA systems. The key features of nuReasoning and its distinctions from prior datasets are illustrated in Fig. 1.

Experiments show that nuReasoning provides consistent benefits across both reasoning and planning. Fine-tuning VLMs on nuReasoning substantially improves driving-specific visual question answering, especially for spatial grounding, decision-making, and counterfactual assessment. Incorporating reasoning supervision into VLA training further improves planning performance, indicating that reasoning annotations can serve as useful intermediate supervision for learning better planning representations. The main contributions of this paper are summarized as:

1. We introduce **nuReasoning**, to the best of our knowledge, the first large-scale real-world dataset focused on long-tail driving scenarios with comprehensive reasoning annotations spanning spatial, decision, and counterfactual reasoning.

2. We propose the **nuReasoning Benchmark**, which evaluates both reasoning and planning performance, providing a unified testbed for VLMs, VLA models, and end-to-end driving models.
3. We benchmark several representative VLMs and planning models, and introduce **nuVLA**, a strong VLA baseline for autonomous driving. Results show that reasoning supervision from nuReasoning consistently improves both VLM reasoning ability and VLA planning performance.

2 Related Work

End-to-end AD. End-to-end driving models replace modular pipelines with unified sensor-to-action learning. Representative methods include UniAD [16], VAD [13], ParaDrive [63], SparseDrive [64], DiffusionDrive [17], and BevAD [65]. Although these methods have substantially advanced end-to-end perception, prediction, and planning, their supervision is still largely dominated by trajectories and detections, limiting their ability to learn explicit reasoning in ambiguous and long-tail scenarios.

Vision-Language-Action Models for AD. Building on the end-to-end driving paradigm, recent VLA models incorporate language into scene understanding, decision-making, and planning. Representative works include DriveVLM [66], SimLingo [67], Orion [68], AutoVLA [33], OpenDriveVLA [34], Alpamayo [35], and Reasoning-VLA [69]. More recent reasoning-oriented methods highlight the importance of reasoning: S4-Driver [29] emphasizes spatial-temporal reasoning, SpaceDrive [59] improves spatial awareness, Counterfactual VLA [61] introduces self-reflective counterfactual reasoning, and OmniDrive [27] bridges planning and language-based counterfactual reasoning. While these works demonstrate the promise of reasoning-centric driving, progress remains constrained by the lack of datasets and benchmarks that systematically support and evaluate diverse reasoning abilities. nuReasoning addresses this gap by providing supervision and evaluation for spatial-temporal, decision, and counterfactual reasoning, and measuring their impact on planning.

AD Datasets and Benchmarks. Large-scale datasets such as nuScenes [42], Waymo Open Motion Dataset [44], and Argoverse [70] have driven progress in perception, forecasting, and simulation. For planning, nuPlan provides a large-scale real-world benchmark [47, 62], while NAVSIM focuses on end-to-end driving evaluation [71, 72]. WOD-E2E [48] extends the data landscape toward long-tail end-to-end driving but lacks reasoning supervision. For closed-loop driving evaluation, CARLA-based benchmarks such as Bench2Drive provide standardized testbeds [73–75]. In contrast, nuReasoning targets long-tail scenarios at scale and introduces structured reasoning annotations with a comprehensive reasoning and planning benchmark.

Reasoning Annotations and Benchmarks. Recent work introduces language supervision through question answering, instruction following, and VLA-oriented annotation. DriveLM [26], MetaVQA [76], LingoQA [53], NuScenes-QA [52], WaymoQA [55], and nuPlan-QA [51] cast driving understanding as QA, while nuInstruct [77] extends this paradigm with multimodal instruction-following. Benchmarks such as DriveBench [24], DVBench [78], and Bench2Drive-VL [79] evaluate VLM reasoning performance. CoVLA [56] provides large-scale trajectory-language pairs, and Impromptu VLA [57] focuses on planning-oriented QA and action supervision. While these datasets advance language-grounded driving, they do not systematically cover diverse reasoning formats in long-tail scenarios. In contrast, nuReasoning provides structured supervision for spatial-temporal, decision, and counterfactual reasoning, together with evaluation of their impact on downstream planning.

3 nuReasoning Dataset

3.1 Data Structure

The nuReasoning dataset adopts a clip-based structure in which each clip spans approximately 20 seconds and is sampled at 10 Hz. Instead of treating individual frames as independent samples, each clip serves as the atomic unit for storage, indexing, and annotation. A clip contains synchronized observation data, including multi-view camera images, LiDAR point clouds, sensor calibrations, ego-vehicle state, object-level 3D bounding box annotations, a static vectorized map, traffic light states, the ego route path, and a high-level navigation command. In addition, the nuReasoning dataset provides reasoning annotations at a lower frequency, which capture spatial understanding, higher-level interpretation, and decision-making signals over the course of the clip.

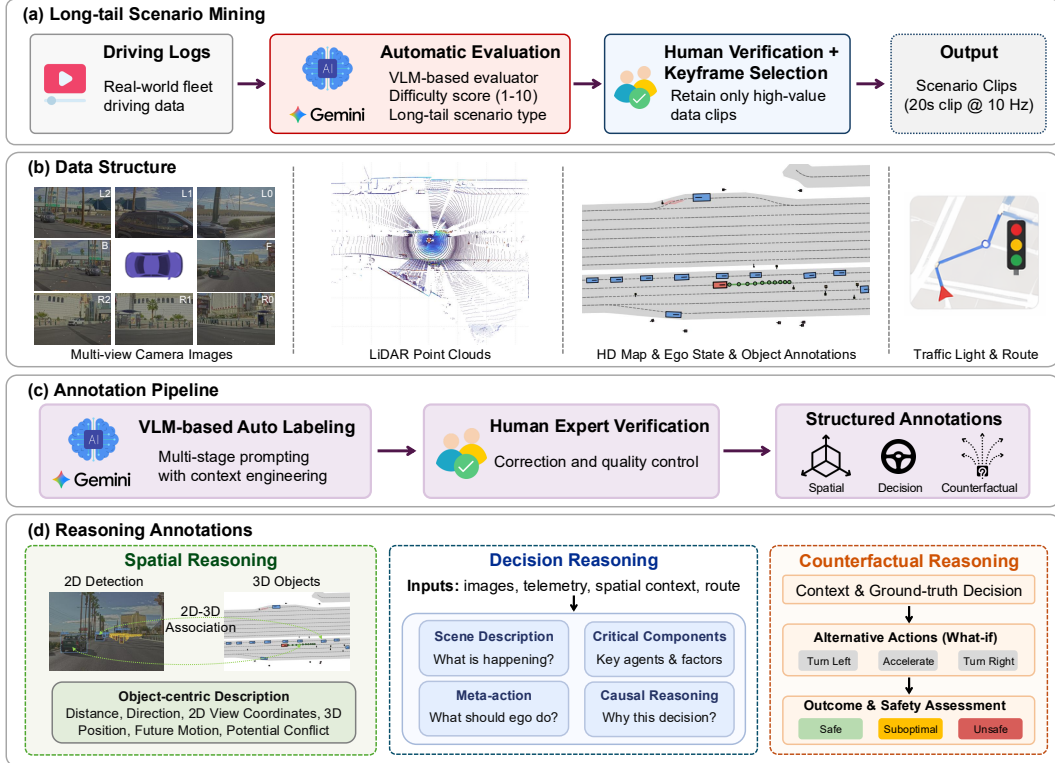


Figure 2: Overview of the long-tail data mining and annotation pipeline. (a) Internal fleet driving logs are segmented and scored by a VLM-based evaluator for scenario type and difficulty, followed by human verification and keyframe selection. (b) Each selected 20-second clip (10 Hz) contains multi-view camera images, LiDAR point clouds, HD maps, ego states, object annotations, traffic lights, and route paths. (c) Annotation combines VLM-based auto-labeling with human verification and correction to ensure quality. (d) Reasoning annotations span spatial, decision-making, and counterfactual dimensions, supporting diverse downstream tasks and reasoning capabilities.

The reasoning annotations are organized into three categories: *Spatial*, *Decision*, and *Counterfactual*. Spatial reasoning describes the scene and the surrounding agents using both image observations from each camera view and 3D geometric information in the ego-centric coordinate system. Decision reasoning explains the intended behavior of the ego vehicle and the basis for that behavior under the observed scene context. Counterfactual reasoning captures the consequences of alternative decisions other than ground-truth actions. In total, the dataset contains 20K clips, which are divided into training, validation, and private test splits. Specifically, 17K clips are used for training, 2K for validation, and 1K clips are reserved as a private test split for challenge evaluation. The overall data processing pipeline, annotation procedure, and dataset structure are illustrated in Fig. 2.

3.2 Data Selection and Processing

We mine Motional’s internal AV fleet driving logs, pre-filtered by the engineering team, to construct a pool of potentially challenging cases, which are segmented into 30-second clips. We develop a VLM-based automatic evaluator, built on Gemini 3.1 Pro, to assess each clip using front-camera data. The evaluator assigns a driving difficulty score from 1 to 10, where 1 denotes nominal driving and 10 denotes highly challenging or rare scenarios, and categorizes each clip into predefined long-tail scenario types, such as vulnerable road users, work zones or roadwork, and perception degradation.

Using this evaluator, we score the candidate pool at scale and retain clips with scores greater than 5 for human verification and keyframe annotation. Human experts review the retained clips, validate their difficulty and long-tail characteristics, and select the decision-critical keyframe following the practice in [35]. Overall, 81.72% of the retained clips are confirmed by experts as long-tail and challenging. For each selected keyframe, we extract 10 seconds of preceding context and 10 seconds of subsequent data to cover both planning history and future scene evolution.

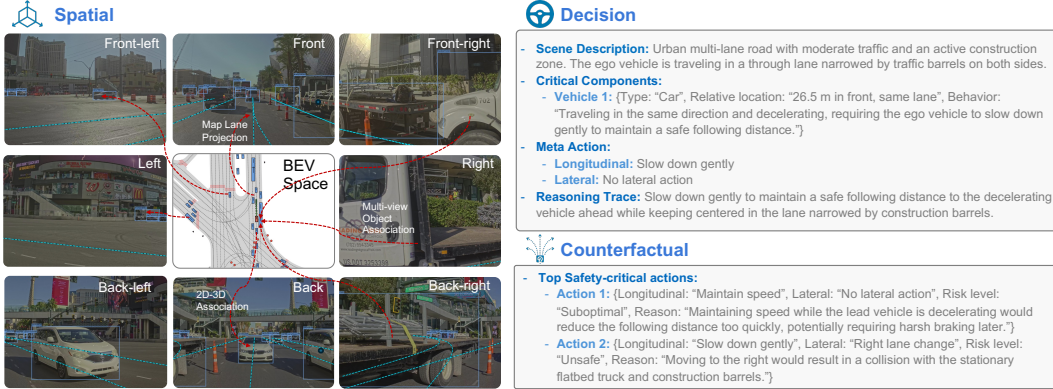


Figure 3: Example of reasoning annotation in the nuReasoning dataset. The frame is annotated with *Spatial*, *Decision*, and *Counterfactual* reasoning to capture scene understanding, meta-actions, and analysis of alternative actions and their risks and outcomes.

All modalities in nuReasoning are synchronized and sampled at 10 Hz, including sensor measurements, object tracks, traffic light states, and ego states. Each clip is paired with a local static vectorized map. We perform reasoning annotation on this curated dataset as described below. Further details on the selection process, evaluator results, and final data distribution are provided in Appendix Section A.

3.3 Reasoning Annotation

We annotate each selected clip with three complementary forms of reasoning: *Spatial reasoning*, *Decision reasoning*, and *Counterfactual reasoning*. Although each clip is centered on a decision-critical keyframe, we annotate multiple frames to capture scene evolution and increase annotation coverage. Spatial reasoning is annotated from 3 seconds into the clip at 1 Hz to track dynamic scene geometry. Decision and counterfactual reasoning are annotated from 5 seconds before the keyframe at 0.2 Hz, matching the lower operating frequency of the decision-making module. Detailed procedures are provided in Appendix Section B, and an annotation example is shown in Fig. 3.

Spatial Reasoning. We use Gemini 3 Flash as a VLM-based 2D detector to identify driving-relevant objects in multi-view images, including dynamic agents and static obstacles. The detected objects are associated with 3D annotated objects via geometric projection and IoU-based matching, yielding cross-view correspondences with ego-centric 3D states (*i.e.*, position, velocity, and category). We then compute semantic relations with respect to the ego vehicle, including distance, lateral and longitudinal relationships, motion state, and potential interaction conflicts. These relations are further augmented with compact map context, such as lane topology and crosswalks.

Decision Reasoning. For each annotated frame, we use synchronized multi-view video observations, ground-truth ego trajectory, spatial reasoning outputs, map context, and route commands to generate decision annotations with Gemini 3.1 Pro, one of the most advanced VLMs for multimodal reasoning. The ground-truth trajectory and video data help align the generated reasoning with the actual driving behavior. Each annotation contains four components: *Scene Description*, *Critical Components*, *Driving Decision*, and *Reasoning Trace*. The driving decision is represented as a structured meta-action with longitudinal and lateral components, and the reasoning trace provides a concise causal justification linking critical agents, route intent, and the selected meta-action. Human experts verify all annotations: automatic annotations achieve 84.69% agreement with experts, and all remaining incorrect annotations are corrected by humans.

Counterfactual Reasoning. At the same timesteps as decision reasoning, we evaluate plausible alternative actions under the same context using Gemini 3.1 Pro. We enumerate meaningful longitudinal and lateral action combinations and classify each alternative as *Safe*, *Suboptimal*, or *Unsafe*, with safety-critical outcomes such as collisions, traffic rule violations, route deviations, or unnecessary blocking explicitly identified. This provides supervision not only for the executed driving action but also for why undesirable alternatives should be avoided. Human experts verify all annotations: automatic counterfactual annotations achieve 76.11% agreement with experts, and all remaining incorrect annotations are corrected by humans.

Table 1: Comparison of **nuReasoning** with representative autonomous driving and reasoning datasets. “*Long-tail*” indicates explicit coverage of rare or challenging scenarios. For reasoning datasets, # Frames refers to annotated frames or timesteps used for reasoning supervision. *Spa*, *Dec*, and *CF* denote spatial, decision, and counterfactual reasoning.

Dataset	Hours	Long-tail	Obj./Map Ann.	Reasoning Ann.	# Frames	Type
nuScenes [42]	5.6	×	Obj. + Map	×	–	–
Argoverse [70]	4.2	×	Obj. + Map	×	–	–
WOD [43]	6.4	×	Obj. + Map	×	–	–
nuPlan (NAVSIM) [47]	120	×	Obj. + Map	×	–	–
WOD-E2E [48]	22.3	✓	×	×	–	–
DriveLM-nuScenes [26]	5.6	×	Obj. + Map	✓	4,871	Spa + Dec
nuPlan-QA [51]	120	×	Obj. + Map	✓	90K	Spa + Dec
CoVLA [56]	83	×	×	✓	100K	Dec
Physical AI AV Dataset [35]	1700	×	Obj.	✓	2,077 [†]	Dec
ImpromptuVLA [57]	144	✓	×	✓	80K	Dec
nuReasoning (ours)	105	✓	Obj. + Map	✓	247K	Spa + Dec + CF

[†]Denotes reasoning labels at distinct annotated timesteps from the publicly available dataset as of May 2026.

VQA Data Generation. We convert the verified structured annotations into VQA pairs grounded in multi-view images and reasoning labels. The questions cover perception, spatial relationships, motion prediction, map understanding, decision-making, and counterfactual risk assessment, with multiple-choice, text-answer, and numerical formats. This process produces more than 10M QA pairs in total. To balance coverage and training efficiency, we subsample 167K QA pairs for training.

3.4 Dataset Statistics

We summarize nuReasoning and compare it with representative AD and reasoning datasets in Table 1. nuReasoning contains 20K clips, totaling approximately 105 hours of curated long-tail driving data collected across multiple U.S. cities, including Las Vegas, Pittsburgh, Los Angeles, and Boston. Each clip is centered on a decision-critical keyframe and includes synchronized multi-modal inputs, object annotations, and local map information. Here, a “frame” denotes a reasoning-annotated timestep; among 19K annotated clips, nuReasoning provides 247K spatial frames sampled at 1 Hz and 57K decision/counterfactual frames sampled at 0.2 Hz. Compared with prior datasets, nuReasoning uniquely combines long-tail coverage, object and map annotations, and comprehensive reasoning supervision spanning spatial, decision, and counterfactual reasoning, enabling evaluation of both reasoning ability and downstream planning.

4 nuReasoning Benchmark

4.1 Reasoning Evaluation

We introduce the reasoning benchmark to evaluate whether VLMs can reason about driving scenes beyond generic visual recognition. Inspired by prior driving VLM benchmarks [26, 51, 24], we group question types by the driving capabilities they assess and report results across four categories: *Geometry*, *Motion*, *Driving*, and *Counterfactual*, which is illustrated in Fig. 4.

Evaluation Metrics. We evaluate each category using the metric attached to its answer format. For multiple-choice categorical questions, we report choice accuracy. For scalar numerical questions, we report tolerance-based accuracy. For coordinate questions, we report the coordinate hit rate and L2 error. For trajectory prediction questions, we report the trajectory hit rate and mean L2 error. For free-form textual reasoning, we report Token-level F1 and ROUGE-L as auxiliary reference-based measures. This follows the common practice in VQA and reasoning benchmarks, while reducing reliance on purely free-form language similarity or LLM-based judging [26, 53, 24, 27].

Evaluation Settings. All models are evaluated using the same testing set and receive the same multi-view, multi-frame camera inputs and textual context. We parse model outputs deterministically: choice answers are normalized to option labels or option text, scalar answers are parsed as numerical

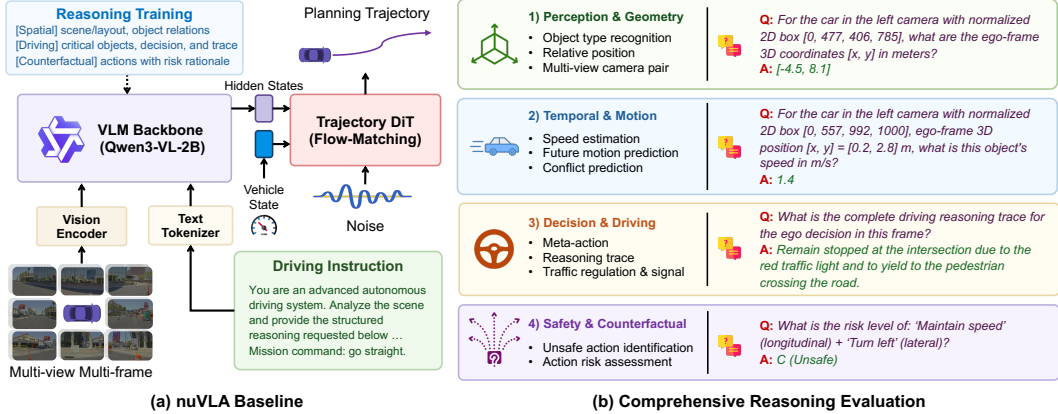


Figure 4: Overview of the nuVLA baseline and the reasoning evaluation benchmark. (a) nuVLA takes multi-view, multi-frame camera images and driving instructions as input. The encoded hidden states are fed into a trajectory DiT to generate future planning trajectories. The VLM backbone is trained with different types of reasoning supervision. (b) For reasoning evaluation, we assess diverse capabilities, including 3D geometric understanding, future object motion estimation, decision-making, and counterfactual reasoning.

values, and coordinate or trajectory answers are parsed into structured numeric outputs. Unparseable outputs are counted as incorrect for tolerance and hit-rate metrics. Detailed settings and the full subcategory mapping are provided in Appendix E.

VLM Baselines. We report both proprietary and open-weight VLM baselines. The proprietary baselines include Gemini-3.1-Pro [80] and Gemini-3-Flash [81]. The open-weight base models include Qwen3.5-4B [82], Qwen3.5-9B [82], and Qwen3-VL-8B-Instruct [83]. We fine-tune these open-weight models using the nuReasoning training dataset and compare the fine-tuned models against their corresponding base models. In addition, we include NVIDIA Cosmos-Reason2-8B [84] as a strong external baseline for zero-shot evaluation.

4.2 Planning Evaluation

We introduce the planning benchmark to evaluate whether driving models can reason over long-tail scenarios and generate appropriate plans. The benchmark assesses the quality of predicted future trajectories under challenging real-world scenarios from the nuReasoning test set.

Evaluation Metrics. We evaluate future ego-planned trajectories using a safety-gated planning score that reflects safety, route-following efficiency, comfort, and behavioral realism. For the key frame in a data clip, the model predicts a trajectory $\hat{\tau} = \{(\hat{x}_t, \hat{y}_t, \hat{\theta}_t)\}_{t=1}^T$, which is compared with the ground-truth future trajectory, HD map geometry, and future states of surrounding objects. We compute normalized scores for non-at-fault collision (NC) s_{NC} , driveable-area compliance (DA) s_{DA} , ego route progress (EP) s_{EP} , comfort (CF) s_{CF} , and human-likeness (HL) s_{HL} . The nuReasoning planning score (NPS) is defined as:

$$NPS = s_{NC}s_{DA} \frac{w_{EP}s_{EP} + w_{CF}s_{CF} + w_{HL}s_{HL}}{w_{EP} + w_{CF} + w_{HL}}, \quad (1)$$

where collision and driveable-area compliance serve as safety gates: unsafe trajectories are strongly penalized before considering progress, smoothness, or imitation quality. We use $w_{EP} = 0.3$, $w_{CF} = 0.2$, and $w_{HL} = 0.5$. We also report average displacement error (ADE) over a 5-second horizon.

VLA Model Baselines. We benchmark various representative VLA baselines, including our proposed strong baseline, **nuVLA**. nuVLA uses a Qwen3-VL-2B vision-language backbone [83] to encode multi-view, multi-frame camera observations and driving context, followed by a flow-matching diffusion Transformer (DiT) head [85] for future trajectory generation. The action head cross-attends to VLM features and predicts a 5-second ego-frame trajectory, which is then evaluated using the planning metrics. The architecture is shown in Fig. 4, with implementation details provided in Appendix Section C. We further include the following VLA baselines. (1) *AutoVLA* [33] is an autoregressive action-generation model that predicts future action tokens sequentially for trajectory

Table 2: Reasoning results under the four main capabilities. Metrics follow the original answer-format evaluation, while the columns are grouped by high-level category. Multi-frame visual input is used as the default setting whenever available. *FT* denotes fine-tuning. *Ch.* is choice accuracy, *Num.* is numerical accuracy within tolerance, *Coord. Hit* and *Traj. Hit* are hit rates for prediction, and *Text F1* is token-level F1; all values are in percentage. *Coord. L2* and *Traj. L2* are the mean L2 errors in task-specific coordinate units. "—" denotes a missing or unparseable trajectory output.

Model	FT	Geometry				Motion				Driving		Counterfactual
		Ch. ↑	Num. ↑	Coord. Hit ↑	Coord. L2 ↓	Ch. ↑	Num. ↑	Traj. Hit ↑	Traj. L2 ↓	Ch. ↑	Text F1 ↑	Ch. ↑
Gemini-3.1-Pro	×	69.2	3.9	2.4	149.80	72.9	12.3	0.0	38.16	54.9	19.7	38.3
Gemini-3-Flash	×	55.6	3.6	2.9	169.74	72.0	11.0	0.0	46.00	52.6	20.0	56.0
Qwen3-VL-8B	×	41.2	2.8	0.1	305.04	71.8	11.7	0.0	138.76	53.6	14.1	44.7
Cosmos-Reason2-8B	×	41.5	2.8	0.0	298.45	68.8	13.1	0.0	77.39	49.1	18.9	46.0
Qwen3-VL-8B	✓	92.0	37.1	46.3	31.38	92.1	25.8	0.0	19.90	70.0	41.9	81.6
Qwen3.5-4B	×	38.8	2.7	0.1	451.27	48.3	5.7	0.0	—	42.6	20.1	47.5
Qwen3.5-4B	✓	92.5	36.9	46.4	25.18	92.2	24.4	0.0	17.36	78.4	42.9	83.3
Qwen3.5-9B	×	47.9	4.6	0.3	212.17	74.9	5.3	0.0	425.68	44.9	19.5	47.2
Qwen3.5-9B	✓	93.3	37.2	52.2	19.53	92.5	25.8	0.2	16.32	74.4	42.6	83.4

Table 3: Comparison of planning models on the nuReasoning test set. *Planning* denotes trajectory planning supervision. nuVLA uses reasoning supervision with different components: S (spatial), D (decision), and CF (counterfactual).

Model	Supervision	Planning Performance						
		NC ↑	DA ↑	EP ↑	CF ↑	HL ↑	NPS ↑	ADE ↓
UniAD [16]	Planning + BEV	88.87	87.62	89.62	92.62	48.80	55.65	2.054
DiffusionDrive [17]	Planning	90.22	88.25	90.46	94.96	51.96	57.86	1.930
AutoVLA [33]	Planning + Decision	90.92	86.48	89.33	99.90	49.89	59.05	2.063
SpanVLA [86]	Planning + Decision	93.78	88.35	85.72	99.80	49.13	60.59	1.890
Alpamayo-1.5 [35]	Zero-shot	90.26	86.13	86.51	97.93	33.79	50.45	2.925
nuVLA	Planning	94.87	92.10	87.38	99.70	55.22	64.98	1.937
nuVLA (D)	Planning + Reasoning (D)	96.25	94.08	90.30	99.90	61.01	70.91	1.676
nuVLA (D + CF)	Planning + Reasoning (D + CF)	96.24	95.36	90.35	99.80	61.26	72.04	1.614
nuVLA (S)	Planning + Reasoning (S)	95.36	92.99	91.52	99.61	61.65	70.64	1.597
nuVLA (S + D)	Planning + Reasoning (S + D)	96.84	94.96	90.55	99.70	60.34	71.63	1.608
nuVLA (S + D + CF)	Planning + Reasoning (S + D + CF)	96.25	96.25	90.73	99.70	62.18	73.09	1.555

planning. (2) *SpanVLA* [86] combines autoregressive reasoning with a flow-matching action expert for trajectory generation. (3) *Alpamayo-1.5* [35] is evaluated in a zero-shot setting to assess transfer from a general-purpose driving model.

End-to-end Baselines. We also include conventional end-to-end driving baselines for comparison. (4) *DiffusionDrive* [17] predicts future ego behavior directly from sensor observations using a diffusion-based planning architecture. (5) *UniAD* [16] is a unified and planning-oriented AD framework for end-to-end perception, prediction, and planning.

5 Experiments

5.1 Implementation Details

All trainable models are trained on 8 NVIDIA A100 GPUs. Each training sample includes multi-view observations from 8 surrounding cameras, with images resized to 448×448 . To incorporate temporal context, we use observations from the previous second across all 8 cameras. For VLM/VLA models, we use a per-GPU batch size of 2 with gradient accumulation over 4 steps, yielding an effective batch size of 64. We fine-tune the vision-language backbone using Low-Rank Adaptation (LoRA). VLA models are trained with AdamW optimizer, with initial learning rates of 1×10^{-4} for the action head and 5×10^{-5} for the VLM backbone. Training uses a linear warm-up followed by cosine annealing. Only samples with reasoning annotations are used for training. Additional details on architecture, training schedules, and hyperparameters are provided in the Appendix.

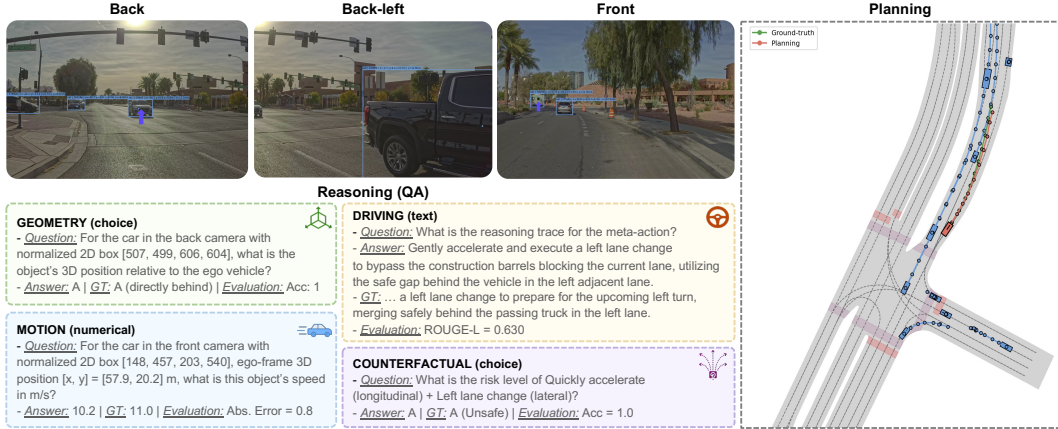


Figure 5: Example of reasoning and planning results on the test set of nuReasoning. Reasoning is evaluated using the fine-tuned Qwen3.5-9B model, while planning is evaluated using the nuVLA model trained with all types of reasoning supervision (S+D+CF).

5.2 Results on Reasoning Benchmark

Results in Table 2 show a substantial gap between generic VLM capability and driving-specific reasoning. Proprietary Gemini models outperform open-weight models on several choice-based metrics, but they remain weak on structured grounding: geometry coordinate hit stays below 3%, and trajectory hit is 0.0% across all base models. This suggests that generic VLM pretraining captures coarse semantic cues but does not reliably learn scene geometry or future motion from multi-view camera inputs. Fine-tuning on nuReasoning improves all four capabilities for open-weight models, and they surpass proprietary models on most metrics. For Qwen3-VL-8B, fine-tuning increases geometry choice accuracy from 41.2% to 92.0%, geometry numerical accuracy from 2.8% to 37.1%, driving choice accuracy from 53.6% to 70.0%, and counterfactual choice accuracy from 44.7% to 81.6%. Similar gains for Qwen3.5-4B and Qwen3.5-9B indicate that improvements are consistent across model scales. Figure 5 provides an example of reasoning and planning outputs.

The main remaining challenge is future motion reasoning. Fine-tuning substantially reduces trajectory L2 error, but strict trajectory hit remains near zero. In contrast, coordinate grounding improves much more strongly, reaching 46.3% for fine-tuned Qwen3-VL-8B and 52.2% for Qwen3.5-9B. This gap suggests that current supervision is sufficient for learning static or instantaneous spatial grounding, but not for precise future motion prediction. Consistent with this interpretation, Cosmos-Reason2-8B [84], despite large-scale pretraining on physical and embodied reasoning [87], remains close to the base Qwen3-VL-8B baseline and does not resolve coordinate or trajectory grounding. These results highlight the importance of fine-grained supervision for task-specific reasoning.

5.3 Results on Planning Benchmark

We train all trainable baseline models on the nuReasoning training set and evaluate them on the test set over a 5 s planning horizon. Alpamayo-1.5 is evaluated in a zero-shot setting. Explicit reasoning outputs are disabled at test time. For nuVLA, ground-truth planning trajectories supervise the trajectory DiT, while diverse reasoning annotations train the VLM backbone; both modules are optimized jointly. As shown in Table 3, nuVLA outperforms competitive end-to-end driving and VLA baselines. Alpamayo-1.5 performs substantially worse under zero-shot evaluation, indicating a clear domain gap between existing VLA models and the long-tail scenarios in nuReasoning.

Adding reasoning supervision consistently improves planning quality over planning-only training. Among individual reasoning sources, spatial and decision reasoning provide strong gains, while counterfactual reasoning offers complementary benefits by exposing the model to unsafe or suboptimal alternatives. Combining spatial, decision, and counterfactual reasoning achieves the best overall performance, suggesting that reasoning supervision improves the learned representations for planning even when explicit reasoning is not generated at inference time.

6 Conclusions

We introduce nuReasoning, a large-scale reasoning-centric dataset and benchmark for long-tail autonomous driving, with structured annotations spanning spatial, decision, and counterfactual reasoning. By jointly evaluating reasoning accuracy and planning performance, nuReasoning fills an important gap in existing AD benchmarks. Experiments show that reasoning supervision improves driving-specific reasoning in VLMs and downstream planning in VLA models, demonstrating its value for building more robust and generalizable AD systems.

Limitations: nuReasoning is collected from a finite set of cities and driving conditions, and may not cover all long-tail scenarios. In addition, the benchmark focuses on open-loop evaluation, which may not fully reflect closed-loop performance.

References

- [1] Shengchao Hu, Li Chen, Penghao Wu, Hongyang Li, Junchi Yan, and Dacheng Tao. St-p3: End-to-end vision-based autonomous driving via spatial-temporal feature learning. In *European Conference on Computer Vision*, pages 533–549. Springer, 2022.
- [2] Zhiqi Li, Wenhai Wang, Hongyang Li, Enze Xie, Chonghao Sima, Tong Lu, Qiao Yu, and Jifeng Dai. Bevformer: learning bird’s-eye-view representation from lidar-camera via spatiotemporal transformers. *IEEE Transactions on Pattern Analysis and Machine Intelligence*, 47(3):2020–2036, 2024.
- [3] Rui Song, Chenwei Liang, Hu Cao, Zhiran Yan, Walter Zimmer, Markus Gross, Andreas Festag, and Alois Knoll. Collaborative semantic occupancy prediction with hybrid feature fusion in connected automated vehicles. In *2024 IEEE/CVF International Conference on Computer Vision and Pattern Recognition (CVPR)*. IEEE/CVF, 2024.
- [4] Zewei Zhou, Hao Xiang, Zhaoliang Zheng, Seth Z Zhao, Mingyue Lei, Yun Zhang, Tianhui Cai, Xinyi Liu, Johnson Liu, Maheswari Bajji, et al. V2XPnP: Vehicle-to-everything spatio-temporal fusion for multi-agent perception and prediction. *Proceedings of the IEEE/CVF International Conference on Computer Vision*, 2025.
- [5] Bencheng Liao, Shaoyu Chen, Xinggong Wang, Tianheng Cheng, Qian Zhang, Wenyu Liu, and Chang Huang. Maptr: Structured modeling and learning for online vectorized hd map construction. In *The Eleventh International Conference on Learning Representations*.
- [6] Zhiyu Huang, Haochen Liu, and Chen Lv. Gameformer: Game-theoretic modeling and learning of transformer-based interactive prediction and planning for autonomous driving. In *Proceedings of the IEEE/CVF International Conference on Computer Vision*, pages 3903–3913, 2023.
- [7] Tianhui Cai, Yun Zhang, Zewei Zhou, Zhiyu Huang, and Jiaqi Ma. Relmap: Enhancing online map construction with class-aware spatial relation and semantic priors. *arXiv preprint arXiv:2507.21567*, 2025.
- [8] Markus Gross, Aya Fahmy, Danit Niwattananan, Dominik Muhle, Rui Song, Daniel Cremers, and Henri Meeß. IPFormer: Visual 3d panoptic scene completion with context-adaptive instance proposals. In *Advances in Neural Information Processing Systems (NeurIPS)*, 2025.
- [9] Daniel Dauner, Marcel Hallgarten, Andreas Geiger, and Kashyap Chitta. Parting with misconceptions about learning-based vehicle motion planning. In *Conference on Robot Learning (CoRL)*, 2023.
- [10] Zhiyu Huang, Zewei Zhou, Tianhui Cai, Yun Zhang, and Jiaqi Ma. Mdg: Masked denoising generation for multi-agent behavior modeling in traffic environments. *arXiv preprint arXiv:2511.17496*, 2025.
- [11] Zhiyu Huang, Xinshuo Weng, Maximilian Igl, Yuxiao Chen, Yulong Cao, Boris Ivanovic, Marco Pavone, and Chen Lv. Gen-drive: Enhancing diffusion generative driving policies with reward modeling and reinforcement learning fine-tuning. In *2025 IEEE International Conference on Robotics and Automation (ICRA)*, pages 3445–3451. IEEE, 2025.

- [12] Li Chen, Penghao Wu, Kashyap Chitta, Bernhard Jaeger, Andreas Geiger, and Hongyang Li. End-to-end autonomous driving: Challenges and frontiers. *IEEE Transactions on Pattern Analysis and Machine Intelligence*, 46(12):10164–10183, 2024.
- [13] Bo Jiang, Shaoyu Chen, Qing Xu, Bencheng Liao, Jiajie Chen, Helong Zhou, Qian Zhang, Wenyu Liu, Chang Huang, and Xinggong Wang. Vad: Vectorized scene representation for efficient autonomous driving. In *Proceedings of the IEEE/CVF International Conference on Computer Vision*, pages 8340–8350, 2023.
- [14] Wenzhao Zheng, Ruiqi Song, Xianda Guo, Chenming Zhang, and Long Chen. Genad: Generative end-to-end autonomous driving. In *European Conference on Computer Vision*, pages 87–104. Springer, 2024.
- [15] Penghao Wu, Xiaosong Jia, Li Chen, Junchi Yan, Hongyang Li, and Yu Qiao. Trajectory-guided control prediction for end-to-end autonomous driving: A simple yet strong baseline. *Advances in Neural Information Processing Systems*, 35:6119–6132, 2022.
- [16] Yihan Hu, Jiazhi Yang, Li Chen, Keyu Li, Chonghao Sima, Xizhou Zhu, Siqi Chai, Senyao Du, Tianwei Lin, Wenhai Wang, et al. Planning-oriented autonomous driving. In *Proceedings of the IEEE/CVF conference on computer vision and pattern recognition*, pages 17853–17862, 2023.
- [17] Bencheng Liao, Shaoyu Chen, Haoran Yin, Bo Jiang, Cheng Wang, Sixu Yan, Xintang Zhang, Xiangyu Li, Ying Zhang, Qian Zhang, et al. Diffusiondrive: Truncated diffusion model for end-to-end autonomous driving. In *Proceedings of the Computer Vision and Pattern Recognition Conference*, pages 12037–12047, 2025.
- [18] Xiaosong Jia, Junqi You, Zhiyuan Zhang, and Junchi Yan. Drivetransformer: Unified transformer for scalable end-to-end autonomous driving. In *The Thirteenth International Conference on Learning Representations*, 2025.
- [19] Bozhou Zhang, Nan Song, Jingyu Li, Xiatian Zhu, Jiankang Deng, and Li Zhang. Future-aware end-to-end driving: Bidirectional modeling of trajectory planning and scene evolution. *arXiv preprint arXiv:2510.11092*, 2025.
- [20] Bozhou Zhang, Jingyu Li, Nan Song, and Li Zhang. Perception in plan: Coupled perception and planning for end-to-end autonomous driving. In *Proceedings of the AAAI Conference on Artificial Intelligence*, volume 40, pages 12376–12384, 2026.
- [21] Haochen Tian, Tianyu Li, Haochen Liu, Jiazhi Yang, Yihang Qiu, Guang Li, Junli Wang, Yinfeng Gao, Zhang Zhang, Liang Wang, et al. Simscale: Learning to drive via real-world simulation at scale. *arXiv preprint arXiv:2511.23369*, 2025.
- [22] Yuping Wang, Shuo Xing, Cui Can, Renjie Li, Hongyuan Hua, Kexin Tian, Zhaobin Mo, Xiangbo Gao, Keshu Wu, Sulong Zhou, et al. Generative ai for autonomous driving: Frontiers and opportunities. *arXiv preprint arXiv:2505.08854*, 2025.
- [23] Tianhui Cai, Yifan Liu, Zewei Zhou, Haoxuan Ma, Seth Z Zhao, Zhiwen Wu, Xu Han, Zhiyu Huang, and Jiaqi Ma. Driving with regulation: Trustworthy and interpretable decision-making for autonomous driving with retrieval-augmented reasoning. In *Proceedings of the AAAI Conference on Artificial Intelligence*, volume 40, pages 38287–38295, 2026.
- [24] Shaoyuan Xie, Lingdong Kong, Yuhao Dong, Chonghao Sima, Wenwei Zhang, Qi Alfred Chen, Ziwei Liu, and Liang Pan. Are vlms ready for autonomous driving? an empirical study from the reliability, data and metric perspectives. In *Proceedings of the IEEE/CVF International Conference on Computer Vision*, pages 6585–6597, 2025.
- [25] Jyh-Jing Hwang, Runsheng Xu, Hubert Lin, Wei-Chih Hung, Jingwei Ji, Kristy Choi, Di Huang, Tong He, Paul Covington, Benjamin Sapp, et al. Emma: End-to-end multimodal model for autonomous driving. *Transactions on Machine Learning Research*, 2025.
- [26] Chonghao Sima, Katrin Renz, Kashyap Chitta, Li Chen, Hanxue Zhang, Chengen Xie, Jens Beißwenger, Ping Luo, Andreas Geiger, and Hongyang Li. Drivelm: Driving with graph visual question answering. In *European conference on computer vision*, pages 256–274. Springer, 2024.

- [27] Shihao Wang, Zhiding Yu, Xiaohui Jiang, Shiyi Lan, Min Shi, Nadine Chang, Jan Kautz, Ying Li, and Jose M Alvarez. Omnidrive: A holistic vision-language dataset for autonomous driving with counterfactual reasoning. In *Proceedings of the computer vision and pattern recognition conference*, pages 22442–22452, 2025.
- [28] Boyi Li, Yue Wang, Jiageng Mao, Boris Ivanovic, Sushant Veer, Karen Leung, and Marco Pavone. Driving everywhere with large language model policy adaptation. In *Proceedings of the IEEE/CVF Conference on Computer Vision and Pattern Recognition*, pages 14948–14957, 2024.
- [29] Yichen Xie, Runsheng Xu, Tong He, Jyh-Jing Hwang, Katie Luo, Jingwei Ji, Hubert Lin, Letian Chen, Yiren Lu, Zhaoqi Leng, et al. S4-driver: Scalable self-supervised driving multimodal large language model with spatio-temporal visual representation. In *Proceedings of the Computer Vision and Pattern Recognition Conference*, pages 1622–1632, 2025.
- [30] Shuhan Tan, Kashyap Chitta, Yuxiao Chen, Ran Tian, Yurong You, Yan Wang, Wenjie Luo, Yulong Cao, Philipp Krahenbuhl, Marco Pavone, et al. Latent chain-of-thought world modeling for end-to-end driving. *arXiv preprint arXiv:2512.10226*, 2025.
- [31] Ming Nie, Renyuan Peng, Chunwei Wang, Xinyue Cai, Jianhua Han, Hang Xu, and Li Zhang. Reason2drive: Towards interpretable and chain-based reasoning for autonomous driving. In *European Conference on Computer Vision*, pages 292–308. Springer, 2024.
- [32] Tianshuai Hu, Xiaolu Liu, Song Wang, Yiyao Zhu, Ao Liang, Lingdong Kong, Guoyang Zhao, Zeying Gong, Jun Cen, Zhiyu Huang, et al. Vision-language-action models for autonomous driving: Past, present, and future. *arXiv preprint arXiv:2512.16760*, 2025.
- [33] Zewei Zhou, Tianhui Cai, Seth Z Zhao, Yun Zhang, Zhiyu Huang, Bolei Zhou, and Jiaqi Ma. Autovla: A vision-language-action model for end-to-end autonomous driving with adaptive reasoning and reinforcement fine-tuning. *arXiv preprint arXiv:2506.13757*, 2025.
- [34] Xingcheng Zhou, Xuyuan Han, Feng Yang, Yunpu Ma, Volker Tresp, and Alois Knoll. Open-drivevla: Towards end-to-end autonomous driving with large vision language action model. In *Proceedings of the AAAI Conference on Artificial Intelligence*, volume 40, pages 13782–13790, 2026.
- [35] Yan Wang, Wenjie Luo, Junjie Bai, Yulong Cao, Tong Che, Ke Chen, Yuxiao Chen, Jenna Diamond, Yifan Ding, Wenhao Ding, et al. Alpamayo-r1: Bridging reasoning and action prediction for generalizable autonomous driving in the long tail. *arXiv preprint arXiv:2511.00088*, 2025.
- [36] Shuang Zeng, Xinyuan Chang, Mengwei Xie, Xinran Liu, Yifan Bai, Zheng Pan, Mu Xu, and Xing Wei. Futuresightdrive: Thinking visually with spatio-temporal cot for autonomous driving. In *The Thirty-ninth Annual Conference on Neural Information Processing Systems*.
- [37] Qihang Peng, Xuesong Chen, Chenye Yang, Shaoshuai Shi, and Hongsheng Li. Colavla: Leveraging cognitive latent reasoning for hierarchical parallel trajectory planning in autonomous driving. *arXiv preprint arXiv:2512.22939*, 2025.
- [38] Qiqi Liu, Huan Xu, Jingyu Li, Bin Sun, Zhihui Hao, Dangen She, Xiatian Zhu, and Li Zhang. Uni-world vla: Interleaved world modeling and planning for autonomous driving. *arXiv preprint arXiv:2603.27287*, 2026.
- [39] Haoyu Fu, Diankun Zhang, Zongchuang Zhao, Jianfeng Cui, Hongwei Xie, Bing Wang, Guang Chen, Dingkang Liang, and Xiang Bai. Minddrive: A vision-language-action model for autonomous driving via online reinforcement learning. *arXiv preprint arXiv:2512.13636*, 2025.
- [40] Yuhang Lu, Jiadong Tu, Yuexin Ma, and Xinge Zhu. Real-ad: Towards human-like reasoning in end-to-end autonomous driving. In *Proceedings of the IEEE/CVF International Conference on Computer Vision*, pages 27783–27793, 2025.
- [41] Hao Shao, Yuxuan Hu, Letian Wang, Guanglu Song, Steven L Waslander, Yu Liu, and Hongsheng Li. Lmdrive: Closed-loop end-to-end driving with large language models. In *Proceedings of the IEEE/CVF conference on computer vision and pattern recognition*, pages 15120–15130, 2024.

- [42] Holger Caesar, Varun Bankiti, Alex H Lang, Sourabh Vora, Venice Erin Liong, Qiang Xu, Anush Krishnan, Yu Pan, Giancarlo Baldan, and Oscar Beijbom. nuscenes: A multimodal dataset for autonomous driving. In *Proceedings of the IEEE/CVF conference on computer vision and pattern recognition*, pages 11621–11631, 2020.
- [43] Pei Sun, Henrik Kretzschmar, Xerxes Dotiwalla, Aurelien Chouard, Vijaysai Patnaik, Paul Tsui, James Guo, Yin Zhou, Yuning Chai, Benjamin Caine, et al. Scalability in perception for autonomous driving: Waymo open dataset. In *Proceedings of the IEEE/CVF conference on computer vision and pattern recognition*, pages 2446–2454, 2020.
- [44] Scott Ettinger, Shuyang Cheng, Benjamin Caine, Chenxi Liu, Hang Zhao, Sabeek Pradhan, Yuning Chai, Ben Sapp, Charles R Qi, Yin Zhou, et al. Large scale interactive motion forecasting for autonomous driving: The waymo open motion dataset. In *Proceedings of the IEEE/CVF international conference on computer vision*, pages 9710–9719, 2021.
- [45] Ming-Fang Chang, John Lambert, Patsorn Sangkloy, Jagjeet Singh, Slawomir Bak, Andrew Hartnett, De Wang, Peter Carr, Simon Lucey, Deva Ramanan, and James Hays. Argoverse: 3d tracking and forecasting with rich maps. In *Proceedings of the IEEE/CVF Conference on Computer Vision and Pattern Recognition (CVPR)*, June 2019.
- [46] Letian Wang, Marc-Antoine Lavoie, Sandro Papais, Barza Nisar, Yuxiao Chen, Wenhao Ding, Boris Ivanovic, Hao Shao, Abulikemu Abuduweili, Evan Cook, et al. Trends in motion prediction toward deployable and generalizable autonomy: A revisit and perspectives. *Foundations and Trends® in Robotics*, 13(1-2):1–269, 2026.
- [47] Holger Caesar, Juraj Kabzan, Kok Seang Tan, Whye Kit Fong, Eric Wolff, Alex Lang, Luke Fletcher, Oscar Beijbom, and Sammy Omari. nuplan: A closed-loop ml-based planning benchmark for autonomous vehicles. *arXiv preprint arXiv:2106.11810*, 2021.
- [48] Runsheng Xu, Hubert Lin, Wonseok Jeon, Hao Feng, Yuliang Zou, Liting Sun, John Gorman, Ekaterina Tolstaya, Sarah Tang, Brandyn White, et al. Wod-e2e: Waymo open dataset for end-to-end driving in challenging long-tail scenarios. *arXiv preprint arXiv:2510.26125*, 2025.
- [49] Seth Z Zhao, Luobin Wang, Hongwei Ruan, Yuxin Bao, Yilan Chen, Ziyang Leng, Abhijit Ravichandran, Honglin He, Zewei Zhou, Xu Han, et al. Bridgesim: Unveiling the ol-cl gap in end-to-end autonomous driving. *arXiv preprint arXiv:2604.10856*, 2026.
- [50] Haibao Yu, Wenxian Yang, Ruiyang Hao, Chuanye Wang, Jiaru Zhong, Ping Luo, and Zaiqing Nie. Drivee2e: Closed-loop benchmark for end-to-end autonomous driving through real-to-simulation. *arXiv preprint arXiv:2509.23922*, 2025.
- [51] Sung-Yeon Park, Can Cui, Yunsheng Ma, Ahmadreza Moradipari, Rohit Gupta, Kyungtae Han, and Ziran Wang. Nuplanqa: A large-scale dataset and benchmark for multi-view driving scene understanding in multi-modal large language models. In *Proceedings of the IEEE/CVF International Conference on Computer Vision*, pages 8066–8076, 2025.
- [52] Tianwen Qian, Jingjing Chen, Linhai Zhuo, Yang Jiao, and Yu-Gang Jiang. Nuscenes-qa: A multi-modal visual question answering benchmark for autonomous driving scenario. In *Proceedings of the AAAI Conference on Artificial Intelligence*, volume 38, pages 4542–4550, 2024.
- [53] Ana-Maria Marcu, Long Chen, Jan Hünemann, Alice Karnsund, Benoit Hanotte, Prajwal Chidananda, Saurabh Nair, Vijay Badrinarayanan, Alex Kendall, Jamie Shotton, et al. Lingoqa: Visual question answering for autonomous driving. In *European Conference on Computer Vision*, pages 252–269. Springer, 2024.
- [54] Yi Gu, Yan Wang, Yuxiao Chen, Yurong You, Wenjie Luo, Yue Wang, Wenhao Ding, Boyi Li, Heng Yang, Boris Ivanovic, et al. Accelerating structured chain-of-thought in autonomous vehicles. *arXiv preprint arXiv:2602.02864*, 2026.
- [55] Seungjun Yu, Seonho Lee, Namho Kim, Jaeyo Shin, Junsung Park, Wonjeong Ryu, Raehyuk Jung, and Hyunjung Shim. Waymoqa: A multi-view visual question answering dataset for safety-critical reasoning in autonomous driving. *arXiv preprint arXiv:2511.20022*, 2025.

- [56] Hidehisa Arai, Keita Miwa, Kento Sasaki, Kohei Watanabe, Yu Yamaguchi, Shunsuke Aoki, and Issei Yamamoto. Covla: Comprehensive vision-language-action dataset for autonomous driving. In *2025 IEEE/CVF Winter Conference on Applications of Computer Vision (WACV)*, pages 1933–1943. IEEE, 2025.
- [57] Haohan Chi, Huan-ang Gao, Ziming Liu, Jianing Liu, Chenyu Liu, Jinwei Li, Kaisen Yang, Yangcheng Yu, Zeda Wang, Wenyi Li, et al. Impromptu vla: Open weights and open data for driving vision-language-action models. *arXiv preprint arXiv:2505.23757*, 2025.
- [58] Weijie Wei, Zhipeng Luo, Ling Feng, and Venice Erin Liong. Spatial-aware vision language model for autonomous driving. *arXiv preprint arXiv:2512.24331*, 2025.
- [59] Peizheng Li, Zhenghao Zhang, David Holtz, Hang Yu, Yutong Yang, Yuzhi Lai, Rui Song, Andreas Geiger, and Andreas Zell. Spacedrive: Infusing spatial awareness into vlm-based autonomous driving. *arXiv preprint arXiv:2512.10719*, 2, 2025.
- [60] Xueyi Liu, Zuodong Zhong, Qichao Zhang, Yuxin Guo, Yupeng Zheng, Junli Wang, Dongbin Zhao, Yun-Fu Liu, Zhiguo Su, Yinfeng Gao, et al. Reasonplan: Unified scene prediction and decision reasoning for closed-loop autonomous driving. In *Conference on Robot Learning*, pages 3051–3068. PMLR, 2025.
- [61] Zhenghao Peng, Wenhao Ding, Yurong You, Yuxiao Chen, Wenjie Luo, Thomas Tian, Yulong Cao, Apoorva Sharma, Danfei Xu, Boris Ivanovic, et al. Counterfactual vla: Self-reflective vision-language-action model with adaptive reasoning. *arXiv preprint arXiv:2512.24426*, 2025.
- [62] Napat Karnchanachari, Dimitris Geromichalos, Kok Seang Tan, Nanxiang Li, Christopher Eriksen, Shakiba Yaghoubi, Noushin Mehdipour, Gianmarco Bernasconi, Whye Kit Fong, Yiluan Guo, et al. Towards learning-based planning: The nuplan benchmark for real-world autonomous driving. In *2024 IEEE International Conference on Robotics and Automation (ICRA)*, pages 629–636. IEEE, 2024.
- [63] Xinshuo Weng, Boris Ivanovic, Yan Wang, Yue Wang, and Marco Pavone. Para-drive: Parallelized architecture for real-time autonomous driving. In *Proceedings of the IEEE/CVF Conference on Computer Vision and Pattern Recognition*, pages 15449–15458, 2024.
- [64] Wenchao Sun, Xuewu Lin, Yining Shi, Chuang Zhang, Haoran Wu, and Sifa Zheng. Sparsedrive: End-to-end autonomous driving via sparse scene representation. In *2025 IEEE International Conference on Robotics and Automation (ICRA)*, pages 8795–8801. IEEE, 2025.
- [65] David Holtz, Niklas Hanselmann, Simon Doll, Marius Cordts, and Bernt Schiele. What matters for scalable and robust learning in end-to-end driving planners? *arXiv preprint arXiv:2603.15185*, 2026.
- [66] Xiaoyu Tian, Junru Gu, Bailin Li, Yicheng Liu, Yang Wang, Zhiyong Zhao, Kun Zhan, Peng Jia, Xianpeng Lang, and Hang Zhao. Drivevlm: The convergence of autonomous driving and large vision-language models. *arXiv preprint arXiv:2402.12289*, 2024.
- [67] Katrin Renz, Long Chen, Elahe Arani, and Oleg Sinavski. Simlingo: Vision-only closed-loop autonomous driving with language-action alignment. In *Proceedings of the Computer Vision and Pattern Recognition Conference*, pages 11993–12003, 2025.
- [68] Haoyu Fu, Diankun Zhang, Zongchuang Zhao, Jianfeng Cui, Dingkan Liang, Chong Zhang, Dingyuan Zhang, Hongwei Xie, Bing Wang, and Xiang Bai. Orion: A holistic end-to-end autonomous driving framework by vision-language instructed action generation. In *Proceedings of the IEEE/CVF International Conference on Computer Vision*, pages 24823–24834, 2025.
- [69] Dapeng Zhang, Zhenlong Yuan, Zhangquan Chen, Chih-Ting Liao, Yinda Chen, Fei Shen, Qingguo Zhou, and Tat-Seng Chua. Reasoning-vla: A fast and general vision-language-action reasoning model for autonomous driving. *arXiv preprint arXiv:2511.19912*, 2025.
- [70] Benjamin Wilson, William Qi, Tanmay Agarwal, John Lambert, Jagjeet Singh, Siddhesh Khandelwal, Bowen Pan, Ratnesh Kumar, Andrew Hartnett, Jhony Kaesemodel Pontes, et al. Argoverse 2: Next generation datasets for self-driving perception and forecasting. *arXiv preprint arXiv:2301.00493*, 2023.

- [71] Daniel Dauner, Marcel Hallgarten, Tianyu Li, Xinshuo Weng, Zhiyu Huang, Zetong Yang, Hongyang Li, Igor Gilitschenski, Boris Ivanovic, Marco Pavone, et al. Navsim: Data-driven non-reactive autonomous vehicle simulation and benchmarking. *Advances in Neural Information Processing Systems*, 37:28706–28719, 2024.
- [72] Wei Cao, Marcel Hallgarten, Tianyu Li, Daniel Dauner, Xunjiang Gu, Caojun Wang, Yakov Miron, Marco Aiello, Hongyang Li, Igor Gilitschenski, Boris Ivanovic, Marco Pavone, Andreas Geiger, and Kashyap Chitta. Pseudo-simulation for autonomous driving. In *Conference on Robot Learning (CoRL)*, 2025.
- [73] Alexey Dosovitskiy, German Ros, Felipe Codevilla, Antonio Lopez, and Vladlen Koltun. Carla: An open urban driving simulator. In *Conference on robot learning*, pages 1–16. PMLR, 2017.
- [74] Xiaosong Jia, Zhenjie Yang, Qifeng Li, Zhiyuan Zhang, and Junchi Yan. Bench2drive: Towards multi-ability benchmarking of closed-loop end-to-end autonomous driving. *Advances in Neural Information Processing Systems*, 37:819–844, 2024.
- [75] Simon Gerstenecker, Andreas Geiger, and Katrin Renz. Fail2drive: Benchmarking closed-loop driving generalization. *arXiv preprint arXiv:2604.08535*, 2026.
- [76] Weizhen Wang, Chenda Duan, Zhenghao Peng, Yuxin Liu, and Bolei Zhou. Embodied scene understanding for vision language models via metavqa. In *Proceedings of the IEEE/CVF Conference on Computer Vision and Pattern Recognition*, pages 22453–22464, 2025.
- [77] Xinpeng Ding, Jianhua Han, Hang Xu, Xiaodan Liang, Wei Zhang, and Xiaomeng Li. Holistic autonomous driving understanding by bird’s-eye-view injected multi-modal large models. In *Proceedings of the IEEE/CVF Conference on Computer Vision and Pattern Recognition*, pages 13668–13677, 2024.
- [78] Tong Zeng, Longfeng Wu, Liang Shi, Dawei Zhou, and Feng Guo. Are vision llms road-ready? a comprehensive benchmark for safety-critical driving video understanding. In *Proceedings of the 31st ACM SIGKDD Conference on Knowledge Discovery and Data Mining V. 2*, pages 5972–5983, 2025.
- [79] Xiaosong Jia, Yuqian Shao, Zhenjie Yang, Qifeng Li, Zhiyuan Zhang, and Junchi Yan. Bench2drive-vl: Benchmarks for closed-loop autonomous driving with vision-language models. *arXiv preprint arXiv:2604.01259*, 2026.
- [80] Google DeepMind. Gemini 3.1 pro model card. <https://deepmind.google/models/model-cards/gemini-3-1-pro/>, 2026. Accessed: 2026-05-01.
- [81] Google, DeepMind. Gemini 3 flash model card. <https://storage.googleapis.com/deepmind-media/Model-Cards/Gemini-3-Flash-Model-Card.pdf>, 2025. Accessed: 2026-05-01.
- [82] Qwen Team. Qwen3.5-omni technical report. *arXiv preprint arXiv:2604.15804*, 2026.
- [83] Shuai Bai, Yuxuan Cai, Ruizhe Chen, Keqin Chen, Xionghui Chen, Zesen Cheng, Lianghao Deng, Wei Ding, Chang Gao, Chunjiang Ge, et al. Qwen3-vl technical report. *arXiv preprint arXiv:2511.21631*, 2025.
- [84] NVIDIA. Cosmos-reason2: Physical ai common sense and embodied reasoning models. <https://huggingface.co/nvidia/Cosmos-Reason2-8B>, 2025. Model card.
- [85] Johan Bjorck, Fernando Castañeda, Nikita Cherniadev, Xingye Da, Runyu Ding, Linxi Fan, Yu Fang, Dieter Fox, Fengyuan Hu, Spencer Huang, et al. Gr00t n1: An open foundation model for generalist humanoid robots. *arXiv preprint arXiv:2503.14734*, 2025.
- [86] Zewei Zhou, Ruining Yang, Xuwei Qi, Yiluan Guo, Sherry X. Chen, Tao Feng, Kateryna Pistunova, Yishan Shen, Lili Su, and Jiaqi Ma. Spanvla: Efficient action bridging and learning from negative-recovery samples for vision-language-action model. *arXiv preprint arXiv:2604.19710*, 2026.
- [87] Alisson G. Azzolini, Hannah Brandon, Prithvijit Chattopadhyay, Huayu Chen, Jinju Chu, Yin Cui, Jenna Diamond, Yifan Ding, Francesco Ferroni, Rama Govindaraju, et al. Cosmos-reason1: From physical common sense to embodied reasoning. *arXiv preprint arXiv:2503.15558*, 2025.

nuReasoning Supplementary Material

A Scenario Evaluation

We develop an automatic scenario evaluation pipeline to identify high-value long-tail driving clips from pre-filtered driving logs. The logs are segmented into 30-second clips at 1 Hz using only front-facing camera views. A VLM-based evaluator is then applied to jointly reason about scene context and ego-vehicle behavior over time.

Prompt for long-tail scenario evaluation (Part I): Scenario taxonomy and evaluation principle.

Scenario type definitions:

- **normal_driving**: no unusual agents, objects, infrastructure, or conditions of safety relevance.
- **abnormal_vehicle_behavior**: unsafe or unexpected vehicle motion (*e.g.*, cut-ins, swerves, harsh braking, U-turns, wrong-way, reversing into traffic).
- **stationary_vehicle_obstruction**: stopped or parked vehicles obstructing or narrowing the lane (*e.g.*, stalled car, double-parking, loading/unloading in lane, doors opening).
- **vulnerable_road_user**: pedestrians, cyclists, micro-mobility, wheelchairs, crowds, or children in or near the roadway in risky positions or motions.
- **animal_on_road**: animals on or crossing the roadway or immediately adjacent in a way that may affect the ego vehicle.
- **road_obstacle_or_debris**: discrete objects in or near the drivable path (*e.g.*, cargo, tire pieces, branches, cones/barrels acting as obstacles, snow piles intruding into lane).
- **road_surface_hazard**: hazardous surface conditions (*e.g.*, potholes, cracks, sinkholes, standing water, flooding, ice, mud, oil).
- **work_zone_or_roadwork**: construction or maintenance altering normal layout (*e.g.*, lane shifts, closures, detours, temporary geometry not in map).
- **traffic_control_or_signage_anomaly**: unusual or faulty signs, signals, or traffic control (*e.g.*, dark-/flashing signals, missing/contradictory signs, manual traffic director, malfunctioning gates).
- **unusual_traffic_pattern**: atypical flow patterns (*e.g.*, unexpected gridlock, contraflow, irregular queues/merging, chaotic flows in semi-structured areas).
- **limited_visibility_or_perception_degradation**: reduced perception due to environment or occlusion (*e.g.*, fog, heavy rain, glare, night, tunnels, strong shadows, occluded intersections, spray on sensors).
- **static_infrastructure_constraint**: fixed geometry or clearance limits (*e.g.*, low bridges/tunnels, narrow lanes, overhanging structures/trees constraining vehicle envelope).
- **emergency_vehicle**: emergency vehicles or scenes requiring special yielding or route changes (active lights/sirens, roadside incident).
- **other**: any other safety-relevant scenario not covered above; briefly describe in the observation field.

Critical evaluation principle: Focus on the ego vehicle’s behavior. A scenario is considered high-value long-tail data only if the unusual element(s) cause a clear, non-trivial change in the ego vehicle’s behavior, such as braking, stopping, yielding, lane changes, evasive steering, rerouting, waiting, significant speed reduction, or hesitation due to uncertainty or occlusion. The mere presence of unusual or critical objects is not sufficient. If a critical object is visible but does not influence the ego vehicle’s actions, the scenario should receive a lower score.

Figure S1: Prompt template used for automatic long-tail scenario evaluation and classification. Part I defines the scenario taxonomy and the core principle that clip value is determined primarily by the impact of unusual elements on ego-vehicle behavior.

Prompt. We design a structured vision-language prompt using Gemini 3.1 Pro to determine whether a clip contains rare or safety-critical driving behavior. The prompt guides the model through chain of thought reasoning: (1) describing the scene, (2) summarizing the ego vehicle’s longitudinal and lateral behavior, (3) identifying unusual or rare elements, and (4) assessing whether these elements materially influence the ego vehicle.

A key design principle is the *behavior-centric criterion*: the presence of rare objects alone is insufficient unless it induces a non-trivial behavioral response from the ego vehicle, such as braking,

yielding, lane changing, evasive steering, waiting, or significant speed reduction. Scenario categories are defined in Fig. S1, and the full prompt template is provided in Fig. S2.

The evaluator produces a structured JSON output containing: (1) scene observations, (2) identified unusual elements, (3) safety assessment, (4) rarity assessment, (5) scenario type labels, and (6) a long-tail value score ranging from 1 to 10. Scores of 1-2 correspond to routine driving, 3-4 to noteworthy but behaviorally irrelevant conditions, 5-6 to meaningful behavioral responses, 7-8 to safety-critical interactions, and 9-10 to extremely rare events involving imminent collision risk or highly atypical hazards. Scenario types include normal driving, abnormal vehicle behavior, stationary vehicle obstruction, vulnerable road users, animals, road debris, surface hazards, work zones, traffic-control anomalies, unusual traffic patterns, limited visibility, infrastructure constraints, emergency vehicles, and other safety-relevant cases.

Prompt for long-tail scenario evaluation (Part II): Reasoning steps, output schema, and scoring rubric.

Reasoning steps:

1. **Scene Description:** Describe the road environment, lighting, weather, and visible agents or objects.
2. **Ego Behavior Summary:** Describe the ego vehicle’s speed profile, lateral behavior, and right-of-way behavior. Explicitly state if ego behavior is unchanged or typical.
3. **Identify Unusual Elements and Ego Influence:** For each unusual element, state whether it changes the ego vehicle’s behavior.
4. **Assess Safety Criticality:** Evaluate how safety-critical the scenario is for ego decision-making.
5. **Determine Rarity:** Assess how rare the scenario is in standard driving datasets.
6. **Final Assessment:** Provide a final score driven primarily by ego behavior impact, then by rarity.

Required JSON output fields:

- **observation:** scene description
- **unusual_elements:** unusual elements and whether they influenced ego
- **safety_assessment:** safety criticality for ego decision-making
- **rarity_assessment:** rarity in standard datasets
- **scenario_types:** one or more scenario types from the predefined list
- **score:** integer from 1 to 10

Scoring rubric:

- **1-2:** Normal driving; no unusual elements; ego behavior typical or unchanged.
- **3-4:** Mildly unusual objects or conditions are present, but they do not materially affect ego behavior or safety margin.
- **5-6:** Moderately long-tail scenario; unusual agents, infrastructure, visibility, or traffic patterns require a clear behavioral adjustment from the ego vehicle, such as yielding, slowing, stopping, rerouting within the lane, or maintaining an increased safety buffer, but without immediate near-conflict.
- **7-8:** High-value long-tail scenario; ego must actively manage elevated risk, such as strong braking, evasive lane change, negotiation with vulnerable road users, occluded hazards, or complex multi-agent interaction.
- **9-10:** Extremely rare and safety-critical scenario; imminent collision risk, severe rule conflict, or highly atypical hazards require immediate, non-standard handling.

Figure S2: Part II of the automatic long-tail evaluation prompt. It specifies the reasoning procedure, structured JSON output, and score definitions used to assess the value of each clip.

Results. We apply the evaluator to more than 100K candidate 30-second clips, and these clips come from drive logs that have been filtered to include challenging cases. We summarize the resulting scenario categories and long-tail value scores in Fig. S3. Overall, the score distribution is heavily skewed toward routine driving. The scenario-type distribution further shows that normal driving remains the largest category, followed by work zones/roadwork and limited visibility. Other long-tail categories, including vulnerable road users, unusual traffic patterns, and stationary vehicle obstruction, occur less frequently but are often more behaviorally significant for the ego vehicle. These results suggest that the evaluator effectively separates common driving clips from a smaller subset of high-value long-tail scenarios.

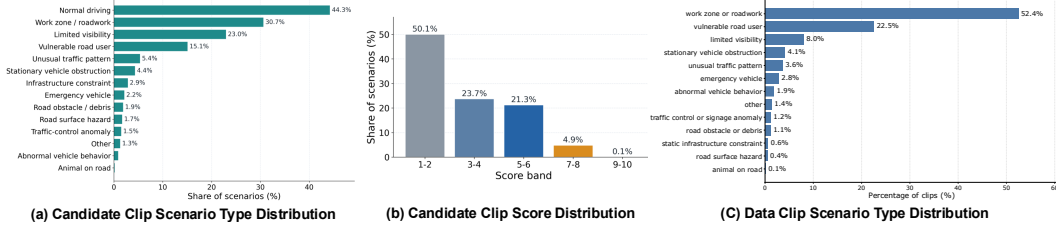


Figure S3: Distribution of scenario evaluation results over candidate clips. (a) Scenario type distribution produced by the VLM-based evaluator on the candidate clips. (b) Distribution of long-tail value scores on the candidate clips. (c) Scenario type distribution of the final data clips.

Human verification. A human expert reviews a subset of the evaluated clips to validate whether each scenario qualifies as a long-tail event and whether the assigned scenario type labels are correct. A second expert independently double-checks the annotations to improve consistency and reduce subjective bias. In addition, the annotators select a *key frame* within each clip, defined as the moment at which a driving decision should be made (e.g., the onset of braking, yielding, or evasive maneuvering). The scenario distribution of the final data clips is shown in Fig. S3.

B Reasoning Annotation

We augment each target frame with structured reasoning annotations that explain the realized ego trajectory in terms of scene constraints, driving actions, and counterfactual alternatives. The annotation pipeline integrates synchronized multi-view camera observations, ego telemetry, map context, object-level spatial relations, and the future ego trajectory.

B.1 Spatial Reasoning Annotation

The spatial annotation stage constructs an ego-centric representation of the scene. For each target timestep, we process multi-camera observations and associate detected image objects with 3D annotations using projected bounding-box overlap. Each matched object is assigned a track token, semantic category, 2D image observations, 3D position in the ego frame, velocity, and a semantic spatial relation to the ego vehicle.

We further enrich each object with temporal and interaction attributes. Future object trajectories are obtained from subsequent annotations when available, or approximated using a constant-velocity model otherwise. Based on these trajectories, we compute interaction metrics including path intersection, time-to-collision, footprint overlap, minimum distance, and conflict type. In addition, nearby map elements such as lane centerlines and crosswalks are selected, represented in the ego frame, and projected into camera views.

B.2 Driving Reasoning Annotation

The driving reasoning stage converts spatial context into a structured explanation of the ego vehicle’s behavior. The annotator takes as input ego velocity and acceleration, high-level navigation commands, temporal camera context, structured spatial annotations, and the future ego trajectory. The future trajectory serves as the reference for action selection, while past and current observations are used to identify the constraints that explain this behavior.

Each driving annotation consists of four components: *scene description*, *critical components*, *driving decision*, and *reasoning trace*. Critical components include only the objects or conditions that directly constrain the maneuver, such as traffic lights, stop signs, pedestrians, leading vehicles, lane blockages, road geometry, construction, visibility limitations, or route intent.

The driving decision is represented by one longitudinal action and one lateral action selected from a fixed taxonomy. Action selection must match the ground-truth future trajectory, while a priority hierarchy is used solely to explain the causal factors behind the decision: (1) collision avoidance, (2) regulatory compliance, (3) geometry and comfort, and (4) efficiency. The prompt specification is shown in Figs. S4 and S5.

Prompt for decision and counterfactual reasoning annotation (Part I): objective, inputs, and critical-component annotation.

System objective. The model is instructed to act as an autonomous driving safety expert and annotate the realized driving trajectory using camera images, telemetry, and structured spatial context. The output must be a single JSON object with exactly five fields: `Scene description`, `Critical components`, `Driving decision`, `Reasoning trace`, and `Counterfactual action analysis`.

Core objective. The prompt requires identifying the *single most restrictive constraint* in the scene according to a strict safety hierarchy, and then explaining how this constraint leads to the realized trajectory. **The future trajectory is treated as ground truth**; when other inputs appear inconsistent, they are interpreted in a way that justifies the realized path.

Input context. The prompt integrates:

- **Goal:** high-level routing intent (`GO_STRAIGHT`, `TURN_LEFT`, `TURN_RIGHT`);
- **Telemetry:** ego velocity, acceleration, and a 5-second future trajectory in ego coordinates;
- **Spatial context:** object relations, map features, lane structure, and per-camera projections;
- **Camera images:** front, front-left, and front-right temporal sequences.

Goal usage rule. The routing goal provides only high-level intent. When the goal is underspecified, the future trajectory reveals the realized longitudinal and lateral behavior and is used to determine the annotated driving decision.

Conflict-resolution rule. When present, the future trajectory takes precedence over all other modalities. If camera observations, traffic controls, or map context appear inconsistent with the realized path, the scene is interpreted as it must have been for that trajectory to occur.

Scene description. The prompt first requires a concise and objective summary of the driving setting, including road type, traffic condition, traffic control, visibility, and ego placement. This section is descriptive only and must not include reasoning or decision language.

Critical components. The prompt then extracts only those objects, controls, or conditions that *directly force* the realized longitudinal or lateral behavior. Critical components must be identified using only **past and current** observations, not future camera frames or future trajectory. The schema includes:

- **Vehicles:** type, relative location, and behavior (*e.g.*, stopped, slowing, cut-in, merge, reversing);
- **Vulnerable road users:** type, relative location, motion state, and gesture if relevant;
- **Traffic controls:** traffic lights and traffic signs with explicit legal effect;
- **Road events and lane features:** curvature, bumps, narrowing, barriers, lane markings, bus lanes, medians;
- **Routing intent and ego state:** route-following constraints and current ego motion state;
- **ODD factors:** weather, visibility, occlusion, construction, emergency vehicles, school-bus rules.

Spatial grounding rule. For vehicles, vulnerable road users, traffic signs, and collision-relevant ODD elements, the prompt requests detailed relative location when the object appears in the structured scene graph; otherwise only a rough distance qualifier is used. Only directly decision-relevant components are retained.

Critical-component example schema.

```
{"Critical components": {"Vehicle 1": {"Type": "Truck", "Relative location": "18 m in front, right adjacent lane", "Behavior": "Cutting into the ego lane and creating immediate collision risk."}, "Traffic sign 1": {"Type": "Stop", "Relative location": "Front right, directly ahead", "Impact": "Complete stop required before proceeding."}}}
```

Figure S4: Prompt template for decision and counterfactual reasoning annotation. Part I defines the task objective, multimodal inputs, conflict-resolution rule, and the schema used to identify critical scene components that directly constrain the realized trajectory.

The reasoning trace is expressed as a concise, single-sentence causal chain that identifies the dominant constraint, explains how it limits feasible motion, and justifies the selected action.

B.3 Counterfactual Reasoning Annotation

The counterfactual annotation stage evaluates plausible alternative action pairs under the same scene conditions. Rather than exhaustively enumerating all longitudinal–lateral combinations, it focuses on meaningful alternatives that are feasible given the current road layout, constraints, and ego state. These alternatives are categorized into: (1) safe and plausible actions, and (2) safety-critical actions that are suboptimal or unsafe. Each candidate is assigned a risk label (`Safe`, `Suboptimal`, or `Unsafe`) along with a brief causal explanation. Safety-critical alternatives are further ranked by their potential risk, such as collision likelihood, rule violation, or degradation of driving safety. This

Prompt for decision and counterfactual reasoning annotation (Part II): driving decision, reasoning trace, and counterfactual analysis.

Driving decision. The prompt requires selecting exactly one longitudinal action and one lateral action to match the realized future trajectory.

Longitudinal action set. The nine longitudinal actions are: *Remain stopped*, *Quickly come to a stop*, *Gently come to a stop*, *Slow down quickly*, *Slow down gently*, *Quickly accelerate (speed up)*, *Gently accelerate (speed up)*, *Maintain speed*, and *Reverse*.

Lateral action set. The seven lateral actions are: *Slightly move left in the lane*, *Slightly move right in the lane*, *Left lane change*, *Right lane change*, *Turn left*, *Turn right*, and *No lateral action*.

Action-selection rule. The selected actions must first match the ground-truth future motion. The priority hierarchy is then used only to explain *why* that trajectory was taken. A special constraint is that if the longitudinal action is *Remain stopped*, the lateral action must be *No lateral action*.

Priority hierarchy. The prompt organizes causal justification using a four-level hierarchy:

1. **Collision avoidance:** blocked paths, crossing agents, cut-ins, and immediate hazards;
2. **Regulatory compliance:** red lights, stop signs, yield conditions, school-bus and rail-crossing rules;
3. **Geometry and comfort:** curves, bumps, narrow gaps, poor road surface, and limited visibility;
4. **Efficiency:** normal unconstrained progress.

Reasoning trace. The prompt then produces a short, single-sentence logic chain linking the dominant constraint to the realized maneuver. It identifies the highest-priority factor, explains why it constrains motion, and states the chosen action.

Counterfactual action analysis. Finally, the prompt evaluates plausible alternative longitudinal–lateral action pairs using only **past and current** scene information. It does *not* enumerate all 81 combinations, but considers only meaningful alternatives allowed by the current road layout, constraints, and ego state. The alternatives are divided into:

- **Alternative actions:** plausible and safe action pairs only;
- **Top safety-critical actions:** the most dangerous or clearly suboptimal alternatives.

Each candidate pair is annotated with a risk level and a short causal explanation. The allowed risk labels are `Safe` for alternative actions, and `Suboptimal` or `Unsafe` for top safety-critical actions.

Final output format. The final response must contain exactly five fields:

- `Scene description`
- `Critical components`
- `Driving decision`
- `Reasoning trace`
- `Counterfactual action analysis`

and must be returned as a single valid JSON object with no surrounding text or markdown.

Figure S5: Part II of the decision-reasoning prompt. It defines the exact longitudinal and lateral action sets, the priority hierarchy used for causal justification, concise reasoning-trace generation, and structured counterfactual action analysis.

process provides explicit supervision not only for the chosen maneuver but also for why other actions are less appropriate.

B.4 Human Verification

To ensure annotation quality, we adopt a two-stage human verification process. A first expert reviews the driving decisions and counterfactual annotations for correctness. A second expert then audits the first expert’s annotations, validating their accuracy and correcting any remaining errors. This sequential review process improves consistency and reliability.

Table S1 summarizes the quality-control protocol for each major annotation source. The automatic stages provide scalable pre-annotations, while human verification is used to validate, correct, or discard noisy labels before they are included in the final dataset. This design reduces the risk that the benchmark merely reflects the failure modes or stylistic biases of the VLM-based annotation pipeline.

Table S1: Annotation quality control in nuReasoning. Auto-human agreement is measured before human correction. All annotations retained in the final dataset are verified by human experts. “Corrected/filtered” indicates that incorrect annotations are either manually corrected or removed during verification.

Annotation type	Auto-label source	Human verification	Agreement	Action
Scenario difficulty and type	Gemini 3.1 Pro	Expert validation	81.72%	Filtered
Spatial reasoning	Gemini 3 Flash + 2D-3D matching	Expert review and consistency check	–	–
Decision reasoning	Gemini 3.1 Pro	Two-stage expert review	84.69%	Corrected
Counterfactual reasoning	Gemini 3.1 Pro	Two-stage expert review	76.11%	Corrected

B.5 QA Generation

We transform the structured annotations into VQA examples grounded in the `Spatial`, `Driving`, and `Counterfactual` components. The QA generation module produces both multiple-choice and numerical questions. Spatial questions cover object identity, ego-relative 3D position, distance, velocity, 2D bounding-box coordinates, image localization, multi-view correspondence, lane and crosswalk geometry, future motion, and interaction outcomes. Driving questions focus on the joint longitudinal–lateral decision, reasoning trace, traffic rules, critical scene elements, and overall scene understanding. Counterfactual questions assess the safety and risk level of alternative actions.

Each QA instance is augmented with metadata specifying its temporal scope (current frame, historical context, or future prediction) and view requirements. Optional language-model-based rephrasing is applied to diversify question phrasing and generate plausible distractors while preserving the correctness of the ground-truth answers.

Additional annotation examples are provided in Fig. S6, with more dynamic cases available in the supplementary materials.

C nuVLA Model Details

C.1 Model

nuVLA architecture. nuVLA is a vision-language-action model for trajectory-level planning in autonomous driving. It contains two trainable components: a Qwen3-VL-2B-Instruct vision-language backbone and a flow-matching Diffusion Transformer (DiT) action expert. The VLM encodes multi-view, multi-frame camera observations together with a natural-language driving prompt, and is supervised to produce structured driving reasoning. The action expert consumes the VLM prompt-side hidden states, ego dynamics, and ego motion history to generate a future ego trajectory for closed-loop planning evaluation.

Multi-view image input. For each scene, we provide synchronized camera images from eight surrounding views: front, front-left, front-right, left, right, back, back-left, and back-right. The number of temporal input steps is configurable. In our default setting, each sample uses one history timestep together with the current timestep, resulting in up to $2 \times 8 = 16$ images per scene. Users may adjust the temporal window according to the model design, compute budget, and task requirements. All input images are resized to 448×448 before being passed to the Qwen processor. Each image is inserted into the chat prompt with an explicit textual tag indicating both its relative time and camera view, e.g., “ $t = -1$, front camera” or “ $t = 0$ (current), front-left camera”. This design lets the VLM associate visual evidence with both spatial viewpoint and temporal context, rather than treating the image list as an unordered collection.

The prompt describes the model role as an autonomous driving assistant, states that the inputs are multi-view multi-frame observations, and includes the mission command, such as `LANE_FOLLOW`. The prompt then requests structured reasoning in the configured format. Our default format is *spatial-driving*: the model predicts both spatial scene understanding and driving-oriented reasoning.

Reasoning supervision. The spatial reasoning target includes a scene/layout summary and object-centric spatial relations. For nearby or relevant agents, the target may include object category,



Figure S6: Additional examples of nuReasoning annotations across diverse driving scenarios.

ego-frame 3D center, per-camera 2D bounding boxes, distance to the ego vehicle, predicted future conflict indicators such as time-to-collision and minimum distance, and short-horizon future object trajectories. Objects are ordered by distance to the ego vehicle and truncated to a fixed maximum number of items. The driving reasoning target contains a driving-oriented scene description, critical components, a structured driving decision, and a reasoning trace. The decision is decomposed into longitudinal and lateral components, such as maintaining speed, decelerating, stopping, lane following, or steering behavior. In formats that include counterfactual supervision, the target additionally contains alternative safe actions and top safety-critical or unsafe actions, together with risk rationales. This reasoning supervision encourages the VLM to expose planning-relevant intermediate factors rather than only producing a final action.

Vision-language backbone. The VLM backbone is initialized from Qwen3-VL-2B-Instruct and fine-tuned using LoRA adapters. We apply LoRA to the attention and MLP projection modules, including query, key, value, output, gate, up, and down projections. The default LoRA rank is 32, scaling factor is 64, and dropout is 0.1. The model uses bfloat16 training and FlashAttention when available. We use the last-layer hidden states of the VLM as vision-language conditioning features. During training, only the prompt-side hidden states, i.e., the user turn containing image tokens, camera/time labels, mission command, and reasoning instruction, are passed to the action expert.

Action expert. The action expert follows a flow-matching DiT design. It predicts an ego-frame future trajectory $\hat{\tau} = \{(\hat{x}_t, \hat{y}_t, \hat{\theta}_t)\}_{t=1}^T$, where $T = 10$, corresponding to a 5-second horizon at 2 Hz. The trajectory is represented as cumulative future waypoints in the current ego frame, with each waypoint containing longitudinal displacement, lateral displacement, and heading. Before flow-matching training, trajectory dimensions are normalized by fixed scales $(50.0, 20.0, \pi)$ for longitudinal position, lateral position, and heading.

The action expert receives three conditioning sources: VLM hidden states, current ego dynamics, and ego motion history. The ego dynamics are represented as (v_x, v_y, a_x, a_y) . The history trajectory contains past ego poses in the ego frame and is flattened together with ego dynamics into a state token. Future action tokens are produced by an action encoder that combines the noisy trajectory with a sinusoidal timestep embedding.

Diffusion Transformer. The DiT operates on the concatenation of one state token and T action tokens. It uses hidden dimension 512, 12 transformer layers, 8 attention heads, and dropout 0.1. Transformer blocks alternate between cross-attention to VLM features and self-attention over state/action tokens. Each block is conditioned on the flow-matching timestep through adaptive layer normalization. The action-token outputs are decoded by an MLP into trajectory velocity predictions.

C.2 Training

nuVLA is trained with a language reasoning objective and a flow-matching action objective. Given multi-view observations I , driving prompt q , and target reasoning text y , the VLM is supervised by

$$\mathcal{L}_{\text{reason}} = - \sum_i \log p_\phi(y_i | y_{<i}, I, q), \quad (\text{S1})$$

where the loss is computed only on assistant-response tokens.

For the action objective, let x_1 be the normalized ground-truth future trajectory and let $\epsilon \sim \mathcal{N}(0, I)$ be Gaussian noise. We sample a flow-matching time t from a Beta distribution and form

$$x_t = (1 - t)\epsilon + tx_1. \quad (\text{S2})$$

The target velocity field is

$$v^* = x_1 - \epsilon. \quad (\text{S3})$$

The action expert predicts $v_\theta(x_t, t, c)$, where c contains the VLM prompt features, ego dynamics, and ego history trajectory. It is trained with

$$\mathcal{L}_{\text{action}} = \|v_\theta(x_t, t, c) - v^*\|_2^2. \quad (\text{S4})$$

The full objective is

$$\mathcal{L} = \mathcal{L}_{\text{reason}} + \lambda_{\text{action}} \mathcal{L}_{\text{action}}, \quad (\text{S5})$$

with $\lambda_{\text{action}} = 1.0$.

We train for 10 epochs with batch size 2, gradient accumulation of 4, VLM learning rate 5×10^{-5} , action-expert learning rate 1×10^{-4} , weight decay 0.01, warmup ratio 0.05, and gradient clipping at norm 1.0. The planning horizon is 5 seconds at 2 Hz, giving 10 future waypoints.

C.3 Inference

At inference time, nuVLA encodes the multi-view camera observations and driving prompt with the Qwen3-VL backbone. The resulting prompt-side hidden states, together with ego velocity, acceleration, and history trajectory, condition the action expert. The action expert initializes the future trajectory from Gaussian noise, $x_0 \sim \mathcal{N}(0, I)$, and performs Euler integration of the velocity field:

$$x_{k+1} = x_k + \Delta t v_\theta(x_k, t_k, c), \quad (\text{S6})$$

where $\Delta t = 1/K$. We use $K = 5$ inference steps for planning evaluation. The final sample is denormalized using $(50.0, 20.0, \pi)$, and heading angles are wrapped to $[-\pi, \pi]$. The resulting 5-second ego-frame trajectory is passed to the planning benchmark for collision, drivable-area, progress, comfort, human-likeness, and overall planning-score evaluation.

D Planning Benchmark

Planning metric details. For each evaluated clip, we select a key frame and evaluate the predicted future ego trajectory $\hat{\tau} = \{(\hat{x}_t, \hat{y}_t, \hat{\psi}_t)\}_{t=0}^T$ over a 5-second horizon at $\Delta t = 0.1$ seconds, yielding 51 poses including the current pose. Trajectories are represented in the global coordinate frame using ego position and heading. Predictions are interpolated onto this benchmark grid and compared against the ground-truth future ego trajectory, the intended route, the static map, and future annotations of surrounding objects.

No-at-fault collision. The collision score s_{NC} measures whether the predicted ego trajectory causes an at-fault contact with surrounding objects. At each predicted waypoint, we construct the oriented ego bounding box, using the ego footprint and rear-axle-to-center offset, and test the bird’s-eye-view polygon overlap with annotated objects at the corresponding timestep. Any positive overlap is treated as a contact. Objects categorized as vehicles, pedestrians, bicycles, or related dynamic classes are treated as agents; cones, barriers, and other non-agent objects are treated as static objects, while ambiguous “other” classes are ignored.

Each contact is classified using relative geometry and motion. Contacts while the ego is stopped are non-at-fault. Contacts with stopped tracks and active front contacts are at fault. Active rear contacts are non-at-fault. Active lateral contacts are at-fault only when the ego is outside the driveable area or spans multiple lanes. Once a track has been processed as a contact, subsequent overlaps with the same track are ignored. If an at-fault collision occurs with a dynamic agent, we set $s_{\text{NC}} = 0$. If the at-fault collision is with a static object, we assign the partial score $s_{\text{NC}} = 0.5$. If no at-fault collision occurs, $s_{\text{NC}} = 1$.

Driveable-area compliance. The driveable-area score s_{DA} evaluates whether the predicted ego footprint remains within the valid road surface. We build the drivable region \mathcal{D} as the union of lane, intersection, and road-block polygons from the static map, expanded by a 0.5 m buffer. For each predicted waypoint, all four corners of the ego bounding box are checked against \mathcal{D} . Timesteps whose ego footprint lies completely outside the known map extent are skipped, so missing map coverage is not penalized. The score is binary:

$$s_{\text{DA}} = \mathbb{I} \left[\forall t \in \mathcal{T}_{\text{map}}, \text{corners}(\hat{x}_t, \hat{y}_t, \hat{\psi}_t) \subseteq \mathcal{D} \right], \quad (\text{S7})$$

where \mathcal{T}_{map} denotes timesteps evaluated within map coverage.

Ego progress. Ego progress s_{EP} measures whether the ego vehicle advances along the intended route. We construct a route polyline from the mission goal route path, interpolate it, and project the starting point and final predicted point onto the route. The predicted progress is $p_{\text{pred}} = \max(0, q_{\text{pred}} - q_0)$, where q_0 and q_{pred} are the route projection distances of the initial and final predicted points. The ground-truth progress p_{gt} is computed analogously from the final ground-truth point. The score is

$$s_{\text{EP}} = \begin{cases} 1, & p_{\text{gt}} < 0.1, \\ \text{clip} \left(\frac{p_{\text{pred}}}{p_{\text{gt}}}, 0, 1 \right), & \text{otherwise.} \end{cases} \quad (\text{S8})$$

Comfort. The comfort score s_{CF} measures whether the predicted trajectory satisfies fixed smoothness constraints. The trajectory is subsampled to a 0.5 second cadence, while preserving the final point, and differentiated with Savitzky-Golay filters. We estimate longitudinal acceleration, lateral acceleration, acceleration-magnitude jerk, longitudinal jerk, yaw rate, and yaw acceleration. The score is binary and equals 1 only if all quantities remain within their configured bounds over the horizon. Otherwise, $s_{\text{CF}} = 0$.

Human-likeness. Human-likeness s_{HL} measures similarity between the predicted and demonstrated future trajectories using final displacement error. Over the shared horizon, we compute per-step displacement errors and report both ADE and FDE:

$$\text{ADE} = \frac{1}{T} \sum_{t=1}^T \|(\hat{x}_t, \hat{y}_t) - (x_t, y_t)\|_2, \quad \text{FDE} = \|(\hat{x}_T, \hat{y}_T) - (x_T, y_T)\|_2. \quad (\text{S9})$$

Table S2: Question categories in four main reasoning capabilities. Counts are from the private testing set manifest (16,437 evaluable samples in total).

Category	Count	Subcategories
Geometry	6,578	object_xy_position, object_relative_position, object_distance, distance_from_2d_bbox, bbox_center_coordinates_1000, normalized_bbox_coordinates_1000, ego_position_from_2d_bbox, image_region_from_3d_object, camera_view_for_3d_object, closest_object_type, multiview_camera_pair, current_lane_coordinates_2d_1000, nearby_lane_count, nearby_crosswalk_count, nearby_crosswalk_coordinates_2d_1000
Motion	3,172	future_motion_label, future_xy_trajectory, future_path_intersection, future_time_to_conflict_s, conflict_prediction, motion_relation, object_speed
Driving	2,619	driving_decision, driving_reasoning_trace, traffic_regulation_light_state, traffic_regulation_signal
Counterfactual	4,068	unsafe_action_identification, action_risk_assessment

The human-likeness score is derived from FDE with a smoothstep penalty. Let $a = 1.0$ m, $b = 8.0$ m, and $u = (\text{FDE} - a)/(b - a)$. Then

$$s_{\text{HL}} = \begin{cases} 1, & \text{FDE} \leq a, \\ 0, & \text{FDE} \geq b, \\ 1 - u^2(3 - 2u), & \text{otherwise.} \end{cases} \quad (\text{S10})$$

The reason to use this instead of a linear penalty is that it avoids harsh changes near the thresholds. Small errors just above 1 meter are not punished too abruptly, and scores taper gently as they approach the failure threshold.

Aggregation. The overall planning score combines the above metrics as

$$\text{PS} = s_{\text{NCSDA}} \frac{w_{\text{EP}} s_{\text{EP}} + w_{\text{CF}} s_{\text{CF}} + w_{\text{HL}} s_{\text{HL}}}{w_{\text{EP}} + w_{\text{CF}} + w_{\text{HL}}}. \quad (\text{S11})$$

The multiplicative safety gate requires collision-free and driveable-area-compliant behavior before rewarding progress, comfort, and human-likeness. We report the mean planning score across valid clips, together with the mean value of each individual metric and the mean ADE/FDE.

E Reasoning Benchmark

This section provides the evaluation details for the VLM reasoning benchmark introduced in Section 4.1. The benchmark is organized around four main categories: geometry, motion, driving, and counterfactual reasoning. This grouping is used only for analysis and reporting; each individual question is still evaluated with the metric appropriate for its answer format. The question categories and counts for evaluation are shown in Table S2.

Label reliability. nuReasoning reduces reliance on purely free-form text evaluation by using structured answer formats whenever possible. Most questions are evaluated against explicit labels such as object positions, distances, object counts, map-derived lane and crosswalk annotations, traffic-light states, future motion categories, and trajectory or coordinate targets. Counterfactual and driving-decision questions are evaluated as multiple-choice problems with fixed answer sets, which avoids open-ended language judgment. Free-form reasoning traces appear only in the `driving_reasoning_trace` subcategory and are reported with reference-based text metrics as auxiliary signals rather than as the primary basis for our conclusions. The test split is held out from fine-tuning. Overall, this design makes the evaluation less sensitive to language style matching and emphasizes structured, metric-grounded driving reasoning.

Output parsing. Model outputs are parsed deterministically according to the expected answer format. For multiple-choice questions, we normalize the response to either the option label or the option text. For scalar numerical questions, we extract a numeric value and compare it with the annotated

target. For coordinate and trajectory questions, we parse structured numeric outputs into points or waypoint sequences before evaluation. If an output cannot be parsed into the required format, it is counted as incorrect for accuracy, tolerance-based, and hit-rate metrics; error-only summaries exclude predictions only when no valid numeric prediction exists.

Choice and numerical metrics. For multiple-choice questions, we report choice accuracy

$$\text{ACC}_{\text{choice}} = \frac{1}{N_c} \sum_{i=1}^{N_c} \mathbf{1}[\hat{y}_i = y_i], \quad (\text{S12})$$

where \hat{y}_i and y_i denote the predicted and ground-truth choices. For numerical questions, we report tolerance-based numerical accuracy

$$\text{ACC}_{\text{num}} = \frac{1}{N_n} \sum_{i=1}^{N_n} \mathbf{1}[|\hat{v}_i - v_i| \leq \epsilon_i], \quad (\text{S13})$$

where \hat{v}_i is the predicted scalar value, v_i is the ground-truth value, and ϵ_i is a task-specific tolerance.

Coordinate and trajectory metrics. Coordinate metrics are computed in the coordinate system required by each question, including normalized image coordinates, bounding-box coordinates, and ego-frame object coordinates. Given a predicted coordinate $\hat{\mathbf{p}}_i = (\hat{x}_i, \hat{y}_i)$ and ground-truth coordinate $\mathbf{p}_i = (x_i, y_i)$, we report coordinate hit rate and mean L2 error:

$$\text{HIT}_{\text{coord}} = \frac{1}{N_p} \sum_{i=1}^{N_p} \mathbf{1}[\|\hat{\mathbf{p}}_i - \mathbf{p}_i\|_2 \leq \delta_i], \quad \text{L2}_{\text{coord}} = \frac{1}{N_p} \sum_{i=1}^{N_p} \|\hat{\mathbf{p}}_i - \mathbf{p}_i\|_2. \quad (\text{S14})$$

where δ_i is the hit tolerance.

For trajectory prediction, with $\hat{\tau}_i = \{\hat{\mathbf{p}}_{i,t}\}_{t=1}^T$ and $\tau_i = \{\mathbf{p}_{i,t}\}_{t=1}^T$, we report trajectory hit rate:

$$\text{HIT}_{\text{traj}} = \frac{1}{N_r} \sum_{i=1}^{N_r} \mathbf{1}\left[\frac{1}{T} \sum_{t=1}^T \|\hat{\mathbf{p}}_{i,t} - \mathbf{p}_{i,t}\|_2 \leq \eta_i\right], \quad (\text{S15})$$

where η_i is the hit tolerance. We additionally report the trajectory mean L2 errors.

Text metrics. For free-form driving rationales in `driving_reasoning_trace`, token-level F1 and ROUGE-L are used as auxiliary reference-based measures:

$$\text{R-L} = \frac{1}{N_t} \sum_{i=1}^{N_t} \text{ROUGE-L}(\hat{s}_i, s_i), \quad (\text{S16})$$

where \hat{s}_i and s_i are the predicted and reference textual answers. These text metrics are not treated as exact semantic equivalence measures; the main conclusions rely on structured choice, numerical, coordinate, and trajectory metrics.

Tolerance configuration. The tolerances ϵ_i , δ_i , η_i are stored per question in the dataset and follow a unified scheme. For numerical scalars,

$$\epsilon_i = \alpha_i + \rho \cdot |v_i|, \quad \rho = 0.05, \quad (\text{S17})$$

where α_i is a subcategory-specific absolute floor and ρ is a 5% relative slack. Table S3 lists the values used in our experiments.

F Additional Results

This section reports additional evaluation results for nuReasoning. Unless otherwise stated, models are evaluated with multi-frame visual input when available. FT denotes fine-tuning on nuReasoning. Choice Acc. denotes choice accuracy, Num. Acc. denotes numerical accuracy within tolerance, Coord. Hit denotes coordinate hit rate, Traj. Hit denotes trajectory hit rate, F1 denotes token-level F1 score. All accuracy, hit-rate, F1 score, and ROUGE-L values are reported as percentages. L2 errors are reported in task-specific coordinate units.

Table S3: Tolerance values used in numerical accuracy and hit-rate metrics.

Metric	Subcategory	Unit	Tolerance
ACC _{num}	nearby_lane_count	count	$\epsilon = 0$ (exact)
	nearby_crosswalk_count	count	$\epsilon = 0$ (exact)
	object_distance	m	$\alpha = 1.0, \rho = 0.05$
	object_speed	m/s	$\alpha = 1.0, \rho = 0.05$
	future_time_to_conflict_s	s	$\alpha = 0.5, \rho = 0.05$
HIT _{coord}	bbox_center_coordinates_1000	px (0–1000)	$\delta = 8$
	normalized_bbox_coordinates_1000	px (0–1000)	$\delta = 8$
	multiview_center_coordinates_1000	px (0–1000)	$\delta = 8$
	object_xy_position	m	$\delta = 1.0$
HIT _{traj}	future_xy_trajectory	m	$\eta = 1.0$
	nearby_crosswalk_coordinates_2d_1000	px (0–1000)	$\eta = 8$
	current_lane_coordinates_2d_1000	px (0–1000)	$\eta = 8$

F.1 Overall Answer-Format Performance

Table S4 summarizes performance across answer formats. Fine-tuning produces large and consistent gains across categorical, numerical, coordinate, and free-form textual outputs. The greatest improvements occur for structured grounding. For example, Qwen3-VL-8B improves from 0.1% to 46.3% coordinate hit rate after fine-tuning, while Qwen3.5-9B improves from 0.3% to 52.2%. These gains are accompanied by much lower coordinate L2 error.

The proprietary Gemini models achieve stronger zero-shot choice accuracy than most open-weight base models, but they remain weak on structured metric outputs. Both Gemini models obtain less than 3% coordinate hit rate and 0.0% trajectory hit rate. This suggests that strong general VLM ability does not automatically translate into precise spatial grounding for autonomous-driving reasoning.

Trajectory prediction remains the most challenging setting. Fine-tuning substantially reduces trajectory L2 error, but the strict trajectory hit rate remains close to zero. This indicates that trajectory reasoning is not solved by answer-format alignment and remains a useful stress test for future work.

Table S4: Overall answer-format and structured-output metrics. Percentages are reported for accuracies, hit rates, token F1, and ROUGE-L. L2 values are reported in task-specific coordinate units. FT denotes models fine-tuned on the nuReasoning training set.

Model	Choice Acc. \uparrow	Num. Acc. \uparrow	Coord. Hit \uparrow	Coord. L2 \downarrow	Traj. Hit \uparrow	Traj. L2 \downarrow	F1 \uparrow	ROUGE-L \uparrow
Gemini-3.1-Pro	57.2	5.9	2.4	149.80	0.0	38.16	19.7	16.0
Gemini-3-Flash	58.4	5.4	2.9	169.74	0.0	46.00	20.0	15.3
Qwen3-VL-8B	49.9	4.9	0.1	305.04	0.0	138.76	14.1	14.6
Cosmos-Reason2-8B	49.3	5.3	0.0	298.45	0.0	77.39	18.9	15.9
Qwen3-VL-8B (FT)	85.4	34.4	46.3	31.38	0.0	19.90	41.9	40.7
Qwen3.5-4B	44.2	3.4	0.1	451.27	0.0	–	20.1	16.5
Qwen3.5-4B (FT)	87.3	33.9	46.4	25.18	0.0	17.36	42.9	41.2
Qwen3.5-9B	52.4	4.7	0.3	212.17	0.0	425.68	19.5	18.3
Qwen3.5-9B (FT)	87.1	34.5	52.2	19.53	0.2	16.32	42.6	40.8

F.2 Representative Difficult Subcategories

Table S5 compares several difficult subcategories across proprietary VLMs, open-weight base models, Cosmos-Reason2-8B, and fine-tuned Qwen3-VL-8B. The selected subcategories cover geometry, motion, driving decisions, and counterfactual risk assessment.

The results show a clear distinction between answer selection and metric-grounded reasoning. Gemini-3.1-Pro and Gemini-3-Flash are competitive on some choice-style tasks, but both perform poorly on coordinate grounding. For instance, on `bbox_center_coordinates_1000`, Gemini-3.1-Pro obtains 3.7% coordinate hit rate and Gemini-3-Flash obtains 4.7%, while Qwen3-VL-8B (FT) reaches 57.5%.

A similar pattern appears for ego-frame object position, where Qwen3-VL-8B (FT) reaches 31.3% while all base models remain below 1%.

Numerical geometry also benefits strongly from fine-tuning. On `object_distance`, Qwen3-VL-8B improves from 10.0% to 74.9%. Counterfactual risk assessment shows another large gain, increasing from 44.7% to 86.5%. By contrast, future trajectory prediction remains unsolved under the strict hit-rate metric, with all models at 0.0% on the selected trajectory task.

Table S5: Representative difficult subcategories. Values are percentages. Each row reports the metric used for that subcategory.

Category	Subcategory	Metric	Count	Gemini-3.1-Pro	Cosmos-Reason2-8B	Qwen3-VL-8B	Qwen3-VL-8B (FT)
Geometry	<code>object_xy_position</code>	Coord. Hit ↑	466	0.6	0.0	0.0	31.3
Geometry	<code>bbox_center_coordinates_1000</code>	Coord. Hit ↑	617	3.7	0.0	0.2	57.5
Geometry	<code>object_distance</code>	Num. Acc. ↑	451	14.4	8.9	10.0	74.9
Motion	<code>future_xy_trajectory</code>	Traj. Hit ↑	422	0.0	0.0	0.0	0.0
Motion	<code>object_speed</code>	Num. Acc. ↑	330	16.1	16.4	14.5	31.5
Motion	<code>future_time_to_conflict_s</code>	Num. Acc. ↑	198	6.1	7.6	7.1	16.2
Driving	<code>driving_decision_joint</code>	Choice Acc. ↑	1,017	44.4	38.8	41.0	58.4
Counterfactual	<code>action_risk_assessment</code>	Choice Acc. ↑	3,051	37.7	46.5	44.7	86.5

Table S6: Subcategory-level comparison for Qwen3-VL-8B before and after fine-tuning under the default multi-frame setting. Values are percentages. Each row uses the metric appropriate for that subcategory. The best result in each row is bolded.

Capability	Subcategory	Metric	Count	Before FT	After FT
Geometry	<code>object_xy_position</code>	Coord. Hit ↑	466	0.0	31.3
	<code>object_relative_position</code>	Choice Acc. ↑	699	33.5	99.6
	<code>object_distance</code>	Num. Acc. ↑	451	10.0	74.9
	<code>distance_from_2d_bbox</code>	Choice Acc. ↑	713	30.7	71.8
	<code>bbox_center_coordinates_1000</code>	Coord. Hit ↑	617	0.2	57.5
	<code>normalized_bbox_coordinates_1000</code>	Num. Acc. ↑	588	0.0	0.0
	<code>ego_position_from_2d_bbox</code>	Choice Acc. ↑	645	40.2	99.2
	<code>image_region_from_3d_object</code>	Choice Acc. ↑	723	38.5	90.7
	<code>camera_view_for_3d_object</code>	Choice Acc. ↑	580	45.2	95.7
	<code>closest_object_type</code>	Choice Acc. ↑	162	80.2	98.8
	<code>multiview_camera_pair</code>	Choice Acc. ↑	287	64.8	99.0
	<code>current_lane_coordinates_2d_1000</code>	Num. Acc. ↑	173	0.0	0.0
	<code>nearby_lane_count</code>	Num. Acc. ↑	167	0.0	98.2
	<code>nearby_crosswalk_count</code>	Num. Acc. ↑	160	1.2	76.9
	<code>nearby_crosswalk_coordinates_2d_1000</code>	Num. Acc. ↑	147	0.0	0.0
Motion	<code>future_motion_label</code>	Choice Acc. ↑	401	38.2	57.4
	<code>future_xy_trajectory</code>	Traj. Hit ↑	422	0.0	0.0
	<code>future_path_intersection</code>	Choice Acc. ↑	503	97.6	99.0
	<code>future_time_to_conflict_s</code>	Num. Acc. ↑	198	7.1	16.2
	<code>conflict_prediction</code>	Choice Acc. ↑	764	99.6	100.0
	<code>motion_relation</code>	Choice Acc. ↑	554	34.5	100.0
	<code>object_speed</code>	Num. Acc. ↑	330	14.5	31.5
Driving	<code>driving_decision_joint</code>	Choice Acc. ↑	1,017	41.0	58.4
	<code>driving_reasoning_trace</code>	ROUGE-L ↑	1,017	14.6	40.7
	<code>traffic_regulation_light_state</code>	Choice Acc. ↑	488	81.6	88.7
	<code>traffic_regulation_signal</code>	Choice Acc. ↑	97	45.4	97.9
Counterfactual	<code>unsafe_action_identification</code>	Choice Acc. ↑	1,017	44.5	66.9
	<code>action_risk_assessment</code>	Choice Acc. ↑	3,051	44.7	86.5

F.3 Subcategory-Level Effect of Fine-Tuning

Table S6 provides a more detailed before-and-after comparison for Qwen3-VL-8B. The gains are broad rather than concentrated in a single task family. Fine-tuning improves relative-position reasoning, distance estimation, position inference from 2D boxes, camera-view reasoning, nearby-lane counting, traffic signal recognition, motion-relation reasoning, and counterfactual risk assessment.

The largest gains are observed on tasks with constrained structured outputs. For example, `object_relative_position` increases from 33.5% to 99.6%, `ego_position_from_2d_bbox` increases from 40.2% to 99.2%, and `motion_relation` increases from 34.5% to 100.0%. These improvements indicate that the nuReasoning dataset helps the model map visual evidence into the required reasoning schema.

However, several dense coordinate-output tasks remain difficult. In particular, `normalized_bbox_coordinates_1000`, `current_lane_coordinates_2d_1000`, and `nearby_crosswalk_coordinates_2d_1000` remain at 0.0% after fine-tuning. These failures show that fine-tuning improves many structured reasoning skills, but precise normalized coordinate generation and lane/crosswalk geometry still require further modeling improvements.

F.4 Analysis of Planning Results

Table 3 compares nuVLA with representative end-to-end driving and VLA baselines on the nuReasoning test set. Prior methods achieve reasonable performance, but remain less effective on the long-tail scenarios emphasized by nuReasoning. The strongest prior baseline achieves an NPS of 60.59, whereas planning-only nuVLA improves this score to 64.98. In contrast, Alpamayo-1.5 performs poorly in the zero-shot setting, obtaining an NPS of 50.45 and an ADE of 2.925, which suggests a clear domain gap between existing VLA training data and the challenging scenarios in our dataset and benchmark.

Reasoning supervision further improves planning performance over the planning-only nuVLA variant. Decision reasoning increases NPS from 64.98 to 70.91 and reduces ADE from 1.937 to 1.676, indicating that high-level driving intent and action-selection supervision benefit trajectory planning. Spatial reasoning also provides strong gains, improving NPS to 70.64 and ADE to 1.597, suggesting that explicit scene-geometry and motion prediction supervision help the model plan more accurately. Counterfactual reasoning provides complementary benefits when combined with decision reasoning, further improving NPS from 70.91 to 72.04 and reducing ADE from 1.676 to 1.614.

The best overall performance is achieved when spatial, decision, and counterfactual reasoning are combined. The full nuVLA model obtains the highest NPS of 73.09 and the lowest ADE of 1.555, while also achieving the best or near-best results on most safety and progress metrics. These results show that different reasoning types provide complementary supervision: spatial reasoning strengthens scene understanding, decision reasoning improves action selection, and counterfactual reasoning helps distinguish safe actions from unsafe or suboptimal alternatives. Importantly, these gains are obtained even though explicit reasoning outputs are disabled during inference, demonstrating that reasoning annotations improve the learned planning representations.

F.5 Qualitative Results

We provide additional qualitative results for the reasoning and planning performance in Fig. S7.

G Broader Impact and Safeguards

Broader impact. nuReasoning aims to support research on safer autonomous driving in challenging long-tail scenarios. Its spatial, decision, and counterfactual reasoning annotations can help models better understand scene context, anticipate risks, and distinguish safe, unsafe, and suboptimal actions. The benchmark also enables systematic evaluation of reasoning and its effect on planning.

However, nuReasoning is an offline benchmark and is not sufficient evidence for real-world deployment. Models may still fail under unseen cities, weather, sensor setups, traffic rules, or rare scenarios outside the dataset, and may overfit to benchmark-specific open-loop metrics. Systems developed with nuReasoning should therefore undergo additional simulation, safety analysis, and real-world validation before deployment.

Safeguards. Because nuReasoning is built from real-world AV fleet logs, it may contain privacy-sensitive visual information. Before release, we apply privacy-preserving anonymization, including blurring faces and license plates. We also use automated filtering and human expert verification to remove unsuitable samples and improve annotation quality. The dataset is intended for research and benchmark use under the accompanying license, usage terms, and privacy and safety requirements.



Figure S7: Additional qualitative results of reasoning and planning performance. Reasoning is evaluated using the fine-tuned Qwen3.5-9B model, while planning is evaluated using the nuVLA model trained with all types of reasoning supervision (S+D+CF).